POWER SYSTEM ANALYSIS CRITERIA-BASED COMPUTATIONAL EFFICIENCY ENHANCEMENT FOR POWER FLOW AND TRANSIENT STABILITY

BY

SOOBAE KIM

DISSERTATION

Submitted in partial fulfillment of the requirements
for the degree of Doctor of Philosophy in Electrical and Computer Engineering
in the Graduate College of the
University of Illinois at Urbana-Champaign, 2014

Urbana, Illinois

Doctoral Committee:

Professor Thomas J. Overbye, Chair
Professor Peter W. Sauer
Associate Professor Deming Chen
Assistant Professor Alejandro Dominguez-Garcia
Assistant Professor Hao Zhu
Dr. Katherine Davis, PowerWorld Corporation

ABSTRACT

As modern power systems have been operated closer to their security limits, the importance of their static and dynamic security assessments is increasing. However, due to the large-scale nature of an interconnected power system and the nonlinear characteristics of power system equations, computational limits impose severe constraints for such security assessments. It is thus critically important to develop rapid and precise power system analysis tools, which are fundamental for the security evaluations.

In this dissertation, comprehensive approaches to both reduce the computational requirements and to achieve a high level of simulation accuracy are examined for application to power system steady-state solutions and transient stability analyses. Three approaches are proposed and validated, which are a mixed power-flow analysis, a mixed transient stability analysis, and an exciter model complexity reduction.

The first approach, a mixed power-flow analysis, focuses on reducing the computational complexity of the steady-state solution. The approach combines ac and dc power flow models to decrease the number of required computations while still capturing variations in the external system. A high level of accuracy in the targeted central part of the system is achieved using the detailed ac model. The less detailed dc model is used for the external system to reduce computational requirements without neglecting it altogether.

In the second approach, the mixed power-flow analysis is extended to transient stability analysis. This method reduces computational requirements for power system transient stability simulation while retaining important dynamic information. In order to prevent the loss of simulation accuracy, the real power losses ignored by the standard dc model are compensated for in the external system.

Finally, the exciter model complexity reduction approach is presented for further improved transient stability analysis. This topic investigates conditions in which fast modes of the exciter model can be neglected or must be preserved. When the fast modes can be ignored, a simpler model with those modes removed replaces an original model and simulation steps can be increased without numerical stability issues. During a transient simulation, the proposed method switches dynamically between the original model and the reduced model, depending on the switching criterion presented.

To Hyun and Chloe

ACKNOWLEDGMENTS

I would like to express my sincere gratitude first and foremost to my advisor, Professor Thomas Overbye, for his invaluable guidance and support throughout my time at the University of Illinois. It was a great honor for me to have an opportunity of working with him and learning from him. My completion of this dissertation could not have been accomplished without his kind consideration and patience. I also offer my sincere appreciation to Professors Peter Sauer, Deming Chen, Alejandro Dominguez-Garcia, Hao Zhu and Dr. Katherine Davis for serving as members of my doctoral committee and giving valuable comments and suggestions on my research.

I would like to acknowledge the Trustworthy Cyber Infrastructure for the Power Grid (TCIPG) and the Korea Electric Power Corporation (KEPCO) for their support. My gratitude is due to Joyce Mast who helped me in English writing. Also thanks to my friends and colleagues at the University of Illinois and in particular Dr. Sudipta Basu, Dr. Yannick Degeilh, Srikanthan Sridharan, Chris Recio, Trevor Hutchins, Saurav Mohapatra, Siming Guo, Rajesh Bhana, Komal Shetye, Wonhyeok Jang, and Max Liu. And thanks and good luck to all other Team Overbye students, both past and current.

Finally, I would like to thank all of my family for their love and support. My parents Sangdeok Kim and Soonyeol Park and my parents-in-law Keunho Jo and Jungsook Yun have given never-ending encouragement to me. I am also thankful to my brother Kyungmo Kim, my sister-in-law Jiyun Kim and

brother-in-law Hanjin Jo. Last but not least, thanks to my wife Hyun Jo and my daughter Chloe Eunjae Kim for being with me and waiting for me. You are my whole life.

TABLE OF CONTENTS

LIST OF TABLES

LIST OF FIGURES

LIST OF SYMBOLS

$\overline{V_k}$	Complex voltage at bus k
V_k	Voltage magnitude at bus k in per-unit
θ_k	Voltage phase angle at bus k
$\overline{I_k}$	Complex injected current at bus k
P_k	Net injected real power at bus k
Q_k	Net injected reactive power at bus k
Y_{km}	Admittance matrix element corresponding to a line between bus k and bus m
G_{km}	Real part of admittance matrix element Y_{km}
B_{km}	Imaginary part of admittance matrix element Y_{km}
$\underline{J}$	Jacobian matrix
f_k^p	Mismatch equations of real power injection at bus k
f_k^q	Mismatch equations of reactive power injection at bus k
f	Differential equations
g	Algebraic equations
x	Dynamic states
y	Algebraic states
δ_i	Rotor angle position of generator i
ω_i	Rotor angle velocity of generator i
H_i	Inertia constant of generator i
T_{Mi}	Mechanical torque of generator i

T_{Ei}	Electrical torque of generator i
D_i	Damping coefficient of generator i
h	Numerical integration time step

CHAPTER 1

INTRODUCTION

1.1 Motivation

Load demand growth, the open access of the transmission system, and economic operations have pushed the power system closer to stability limits [1]. It is very important for power system control centers to be able to analyze the behavior of the electric power system accurately and quickly to ensure a secure energy delivery system. Such analysis allows the system operators to prepare for unpredictable contingency events such as generator losses, line-switching operations, faults and sudden load changes.

Interconnections within modern power grids have increased the system complexity. The power system is comprised of millions of loads and generators, and tied together by hundreds of thousands of miles of transmission and distribution wires with a myriad of control devices. As a result, to perform a power system simulation for static and dynamic security assessments, we are required to solve a huge number of nonlinear differential and algebraic equations, for every one of the many contingency cases [2]. Recent integration of renewable energy and storage involves additional modeling of non-synchronous, inertia-less and inverter-interfaced sources. Heavy computational demands in terms of storage and simulation time are required. These computational limits impose severe constraints for power system analysis, especially for real-time situational awareness and on-line decision making.

Developing powerful computational tools for fast and accurate power system analysis has been an open challenge for many decades.

1.2 Review of the State of the Art

Many efforts have been made to speed up power system analysis by adapting the increased computing power of hardware and by exploiting more efficient reduction algorithms. Dramatic advancements in microprocessor technology have made substantial improvements of computational efficiency. Moreover, parallel processing technology utilizing multiple hardware components has long been discussed as an approach to greatly enhance solution speed [3, 4]. An earlier implementation can be found in [5] and it was advanced in [6, 7]. Parallel processing allows consideration of a larger number of contingencies, such that multiple scenarios can be studied simultaneously. This achieves fast simulation without simplifying the power system model.

Emphasis on speeding up simulation in power system areas has been primarily directed to developing efficient network reduction algorithms. These approaches partition the electric power system into internal and external systems. The internal system denotes the area of interest for study. The power system model size is decreased by replacing the external system with small equivalents, while the internal system is unchanged. The network reduction techniques are divided into static and dynamic equivalents depending on the system model equations and the purpose. The static equivalent methods aim to reduce a system model for power-flow studies, which is fundamental for operating and planning power systems. The power-flow analysis validates that bus voltage magnitudes are close to rated values, generators operate within specified limits, and transmission lines, transformers, and other equipment

are not overloaded. For the dynamic equivalent, the goal is to reduce the computational demands for transient stability analysis. The objective of such analysis is to determine whether or not power systems will reach a new operating point and to examine how system properties undergo transient deviations from an equilibrium following a disturbance.

1.2.1 Static equivalent approach

Ward equivalents

The classical Ward-type equivalent has been the most widely used and was originally proposed by Ward in [8]. The basic idea is that the external system is eliminated by performing Gaussian elimination on the complex nodal admittance matrix representing the network configuration. The Ward equivalent has two different versions: the *Ward injection* and the *Ward admittance* methods [9]. The difference is only in the ways that the external bus powers are modeled. In the Ward injection method, the injected power at each bus is converted to the injected current as shown in (1.1). After reduction shown in (1.2), the equivalent currents at the boundary buses comprising the boundary between the internal and the external systems are converted back to constant power injections for power-flow studies. Figure 1.1 shows the original system and the reduced system where the whole external system is equivalenced. The Ward admittance method converts all injected powers to shunt admittances such that the external system injections are zero. The equivalent becomes a passive network. In some situations, the Ward admittance method tends to amplify the effect of external shunt admittances at the boundary buses, and unusual shunts in the reduced network result in serious convergence problems. Thus, emphasis is given to the Ward injection method

because of its reliability and attractive properties for on-line application [10].

$$\begin{bmatrix} Y_{ee} & Y_{eb} & 0 \\ Y_{be} & Y_{bb} & Y_{bi} \\ 0 & Y_{ib} & Y_{ii} \end{bmatrix} \begin{bmatrix} V_e \\ V_b \\ V_i \end{bmatrix} = \begin{bmatrix} I_e \\ I_b \\ I_i \end{bmatrix} \tag{1.1}$$

$$\begin{bmatrix} I & {Y_{ee}}^{-1}Y_{eb} & 0 \\ 0 & Y_{bb} - Y_{be}{Y_{ee}}^{-1}Y_{be} & Y_{bi} \\ 0 & Y_{ib} & Y_{ii} \end{bmatrix} \begin{bmatrix} V_e \\ V_b \\ V_i \end{bmatrix} = \begin{bmatrix} {Y_{ee}}^{-1}I_e \\ I_b - Y_{be}{Y_{ee}}^{-1}I_e \\ I_i \end{bmatrix} \tag{1.2}$$

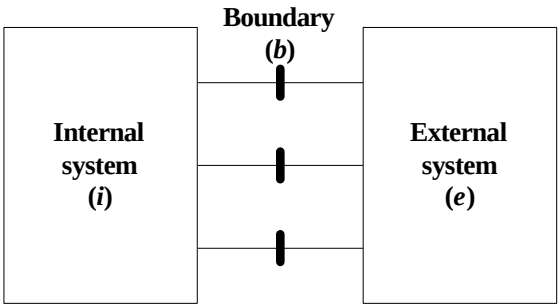

(a) Original system corresponding to (1.1)

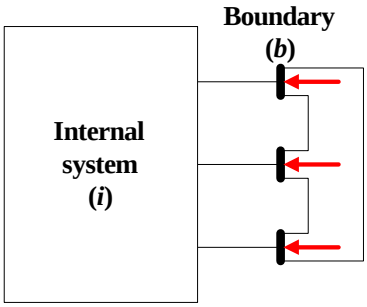

(b) Reduced system corresponding to (1.2)

Figure 1.1: Ward injection method

The Ward equivalent gives reasonably accurate results for MW response, but it has a limitation on representing the VAR response from the external system. It has been modified such that the Gaussian elimination is performed only on external PQ buses. This is referred to as the *Ward-PV equivalent* [11].

Monticelli et al. proposed the *extended Ward equivalent*, which is a Ward equivalent with additional fictitious reactive power support at the boundary buses [12]. The fictitious generator provide no real power. But, it supplies adjustable reactive power to the reduced system. Its reactive power response is close to that of the Ward-PV method.

REI equivalents

Dimo proposed the REI (Radial Equivalent Independent) equivalent, which aggregates the power injections of a group of eliminated buses into a fictitious node, called the *REI node* [13, 14]. This node in the reduced system replaces the corresponding group in the original network. Three basic steps are shown in Fig. 1.2 [10]. The number of REI nodes can be varied depending on desired accuracy for contingency evaluation. For large power systems, between 10 and 100 REI nodes may be required [9]. However, the modeling accuracy of the REI equivalent is strongly dependent on the operating point. For on-line application, it is much less satisfactory in PQ and PV buses than the Ward equivalent.

PTDF-based equivalent

Efficient power system market operations require that market participants are able to analyze market behaviors. Such analysis also demands heavy computation, particularly when performing long-term simulations. In recent years, several new equivalent approaches were proposed for considering characteristics of power market studies. The PTDF-based equivalent correctly approximates the PTDFs (Power Transfer Distribution Factor) and ISFs (Injection Shift Factor) of the original system using the dc power-flow model

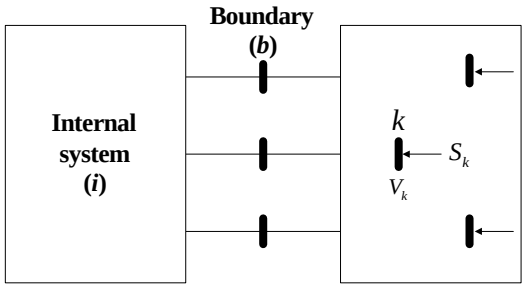

(a) Original system with external injections

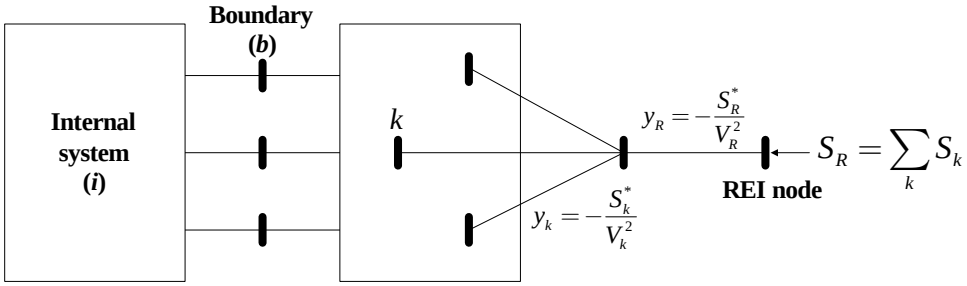

(b) Attached REI network

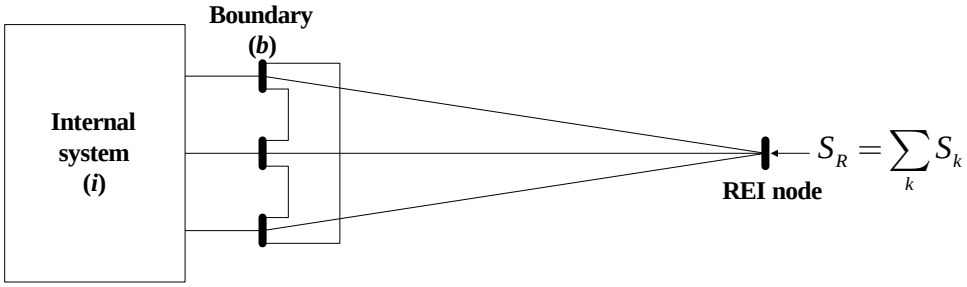

(c) REI equivalent

Figure 1.2: REI equivalent method

[15]. [16] pointed out that the reduced networks of the conventional equivalent method are dependent on the operating point, which produces significant error for a different set point. This is a critical issue for economic and planning studies which need to consider various load and generation profiles. In order to preserve inter-area flows for various operating points, this approach aggregates buses based on the PTDF matrix and optimizes branch values between areas.

1.2.2 Dynamic equivalent approach

The power system model is represented with the nonlinear differential and algebraic equations (DAE) for a transient stability simulation [2]. The internal system is of the following form:

$$\dot{x_{int}} = f_{int}(x_{int}, y_{int}) \tag{1.3}$$

$$0 = g_{int}(x_{int}, x_{bd}, y_{int}, y_{bd}) \tag{1.4}$$

and the external system is of the following form:

$$\dot{x_{ext}} = f_{ext}(x_{ext}, y_{ext}) \tag{1.5}$$

$$0 = g_{ext}(x_{ext}, x_{bd}, y_{ext}, y_{bd}) \tag{1.6}$$

where x denotes the dynamic states, y is the algebraic states, f represents the differential equations such as the swing equation and controller dynamics, g contains stator and network algebraic equations, and subscripts *int*, *bd* and *ext* denote internal, boundary and external systems, respectively.

The dynamic equivalent approach is used to obtain a simplified model which represents the external system for transient stability analysis. Most

of the dynamic equivalent methods were proposed in the 1970s and 1980s when computing resources were limited. However, because there are many problems of modeling a large power system, advanced equivalent techniques are still being developed [17]. The dynamic equivalent models can be categorized broadly into *modal*, *coherency* and *measurement-based* methods [18]. The modal method is based on a linearized model and eliminates unexpected or insignificant modes in the external system. The coherency-based method uses the concept of coherency and aggregation to create reduced models in the form of nonlinear power system models. In the measurement-based method, the external system responses are used to determine the parameters of the simplified equivalent models.

A. Modal method

The modal equivalent method simplifies the external system by the use of a linear model. This would be reasonable because the external system is not perturbed significantly by a disturbance in the internal system. The external system is simply linearized around an operating point.

$$\Delta \dot{x}_{ext} = A\Delta x_{ext} + B\Delta y_{ext} \tag{1.7}$$

$$0 = C\Delta x_{ext} + D\Delta x_{bd} + E\Delta y_{ext} + F\Delta y_{bd} \tag{1.8}$$

where

$$A = \left.\frac{\partial f_{ext}}{\partial x_{ext}}\right|_{x_o,y_o} \quad B = \left.\frac{\partial f_{ext}}{\partial y_{ext}}\right|_{x_o,y_o} \quad C = \left.\frac{\partial g_{ext}}{\partial x_{ext}}\right|_{x_o,y_o}$$
$$D = \left.\frac{\partial g_{ext}}{\partial x_{bd}}\right|_{x_o,y_o} \quad E = \left.\frac{\partial g_{ext}}{\partial y_{ext}}\right|_{x_o,y_o} \quad F = \left.\frac{\partial g_{ext}}{\partial y_{bd}}\right|_{x_o,y_o}$$

The linear model reduces the computational demands. Further compu-

tational decreases were achieved by the following approaches. Undrill et al. developed a modal truncation method in which only the dominant modes are retained for representing the external system with a linear model [19, 20, 21]. This approach eliminates highly damped modes, while extracting the relatively less damped modes. The latter are dominant and include the electromechanical modes. The modal truncation method does not preserve steady-state values, and the retained modes of the reduced model are not identical to the modes of the full external system model.

Another key variant of the linear methods is selective modal analysis which employs the eigenvalues, eigenvectors and participations factors of the linear system [22, 23]. The state variables, which show the high participation factors in the modes of interest, are maintained, and the effects of the less relevant variables are incorporated with approximate equivalent iteratively refined.

B. Coherency method

The most common method used to create the dynamic equivalent is based on the concept of coherency and aggregation. *Coherency* means that some generators closely coupled in an electrical sense exhibit similar rotor angle responses following disturbances. In general, generators i and j are considered to be coherent if the following criterion is satisfied over a certain time interval:

$$|\Delta\delta_i(t) - \Delta\delta_j(t)| < \varepsilon \tag{1.9}$$

where $\Delta\delta_i(t)$ and $\Delta\delta_j(t)$ are the rotor-angle deviations of generators i and j, respectively.

The characteristic behaviors of coherent generators can be exploited to reduce the size of the power system model without significant loss of simulation

accuracy. In the coherency method, the group of generators are aggregated and then converted to a single equivalent machine. This involves three main steps: (1) identification of coherent group of generators, (2) aggregation of each coherent group of generators, and (3) reduction of the external network. The coherent-based equivalents have been extensively studied and there exist many variations in each step of the coherency method.

(1) Coherency identification In coherency identification, the most intuitive approach is to compare the responses of generators from a full nonlinear simulation. When the deviation of machine rotor angle responses is smaller than a specified tolerance (ϵ), certain groups of generators are considered to be tightly coherent. Otherwise, they are weakly coherent. An example of coherency identification is carried out on a 16-machine 68-bus system [24]. Figure 1.3 shows the rotor angle responses of all 16 generators and the group of coherent generators which are identified from the simulation results.

Podmore and Germond proposed linear time simulation method in place of the complicated nonlinear simulation [25, 26]. This approach has an advantage such that the linear simulation is much faster than a full nonlinear simulation. However, the simulation-based methods are still time-consuming. Many direct identifications have been proposed.

Slow coherency based on singular perturbation theory separates the slow and fast dynamics in a system [27, 28]. The slow dynamics arise from the slower inter-area modes, which result from groups of generators on one side of the tie line oscillating against groups of generators on the other side. The evaluation of the coherent groups is based on the set of slow modes and their mode shapes, which are represented by eigenvectors. However, the computation of eigenvalues for the slow coherency method is time consuming for large

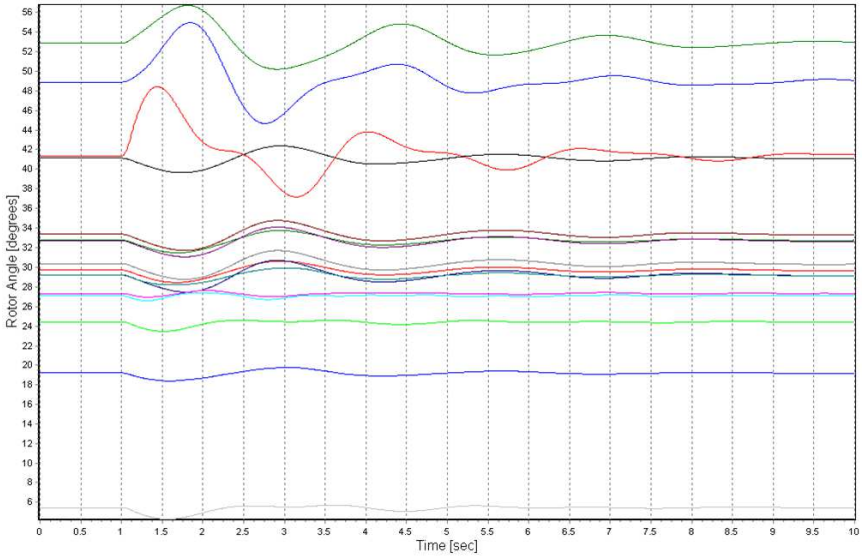

(a) Rotor angle responses

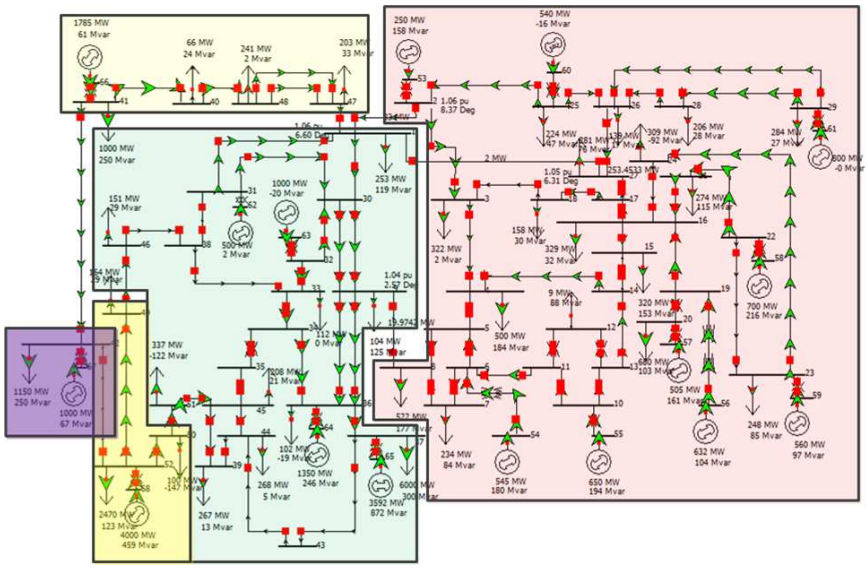

(b) Idenfitied groups of coherent generators

Figure 1.3: Example of coherency identification with the 68-bus system

power systems. In [29], a weak-line method using the system state matrix was proposed to identify the groups of generators. This method iteratively computes a coupling factor from the synchronizing torque coefficients. If the coupling coefficients among the generators are high, that group of generators is considered to be coherent. The method was advanced in [30], which forms both weakly coherent areas and strongly coherent areas.

Generator coherency is dependent on system operating conditions, because the identification is made from a small-signal analysis. When operating conditions are changed, the coherency group might be identified by reevaluating the slow coherency behaviors. In recent years, a systematic approach was developed to predict the change of generator slow coherency with different operating conditions, and to form an appropriate boundary area by including the critical generators, which become a strong coherency with the internal system [31].

(2) Generator aggregation The next procedure is to aggregate the coherent generators in a group, which reduces the number of generators in the external system. The procedure proposed by Germond and Podmore consists of three basic steps, which are shown in Fig. 1.4 [26]. The first step is to connect all the coherent generators to a common bus, an equivalent bus through ideal transformers with complex ratio. The voltage of common bus is defined either an average voltage of the group or the voltage of an individual bus. The branches between coherent buses are replaced by equivalent shunt admittance. The second step is that generators, loads, and shunt admittances are transferred to the equivalent bus. All the generators at the equivalent bus are then converted to a single generator. The constructed equivalent generators preserve the power flows in the original system as well

as the power system model. Aggregated frequency responses with a least square fit are used to approximate machine, exciter and governor function of the equivalent generator. The last step is to eliminate the original coherent buses by combining original branch and the ideal transformer.

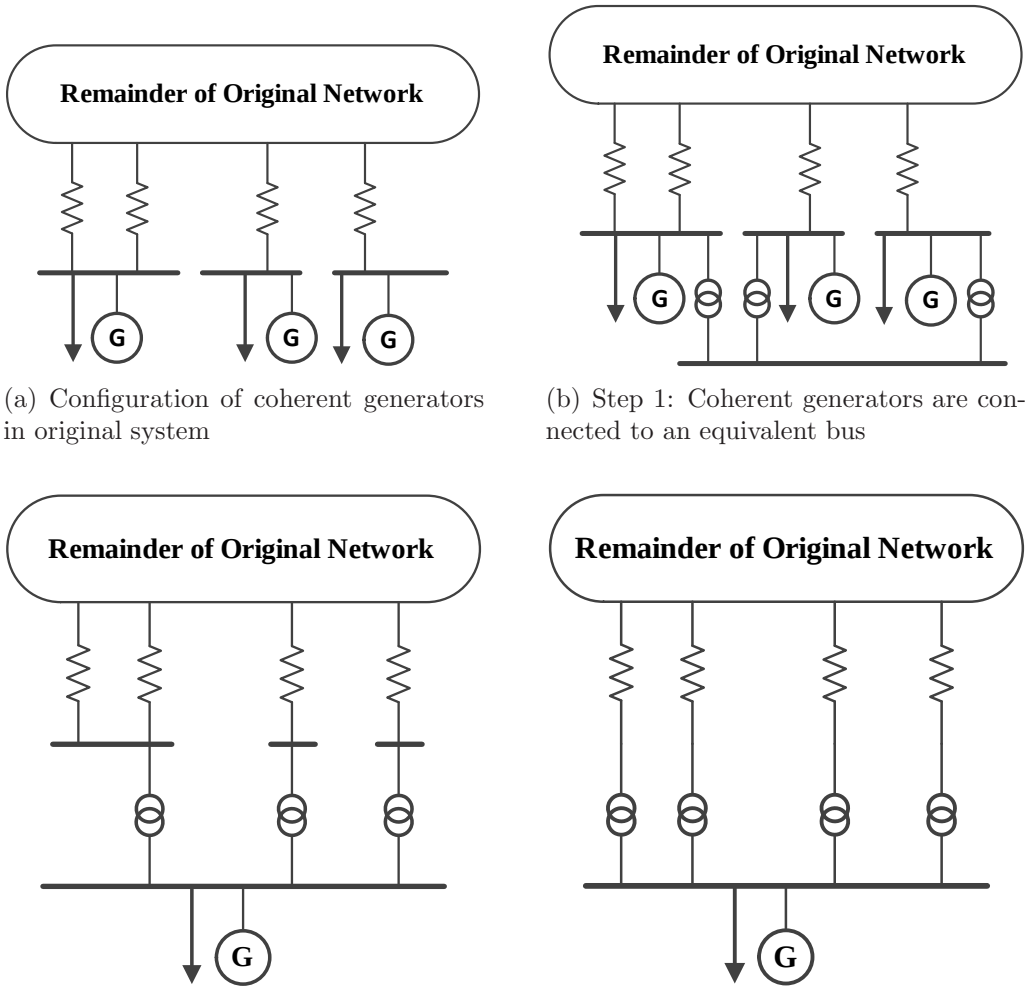

(a) Configuration of coherent generators in original system

(b) Step 1: Coherent generators are connected to an equivalent bus

(c) Step 2: All components are transferred to the equivalent bus

(d) Step 3: Original generator buses are eliminated

Figure 1.4: Generator aggregation method by Podomre and Germond

More advanced aggregation methods were proposed to improve the performance of the reduced model. Those are based on the singular based perturbation theory, which generates asymptotic series expansion terms to enhance

the slow subsystem [32]. The inertial aggregation method aggregates the coherent groups at the generator internal node, rather than at the generator bus. However, the reduced model from the inertial aggregation method introduces a higher inter-area mode frequency in a large power system. Slow coherency aggregation method corrects the problem by connecting finite admittance between the generator buses.

(3) Network reduction The final procedure to derive the coherency-based equivalent is to reduce the external network. The buses with constant impedance loads are eliminated using Gaussian elimination and an exact reduction is possible. Other nonlinear load models consisting of constant current and constant power loads are replaced by appropriate equivalent models and then Gaussian elimination is performed. More details can be found in [28].

C. Measurement-based method

Measurement-based methods have used real-time measurements or simulated responses of the power system to simplify the external network [33, 34, 35]. Conventional measurement-based methods first select an equivalent model structure. The parameters of the selected equivalent model are then estimated by solving optimization problems, which minimize the differences between the responses with the original system and those with the equivalent system. The problem formulation is shown in (1.10). Overall procedure of the parameters estimation is depicted in Fig. 1.5.

$$\underset{p}{\text{minimize}} \quad J(p) = \sum_{i \in B} \sum_{j \in I} (P_{ij}^{original} - P_{ij}^{reduced}(p))^2 \tag{1.10}$$

where the control variable p is the parameters of the selected equivalent

model, B is the set of boundary nodes, I is the set of buses in the internal system and P_{ij} is the real power-flow from bus i and j.

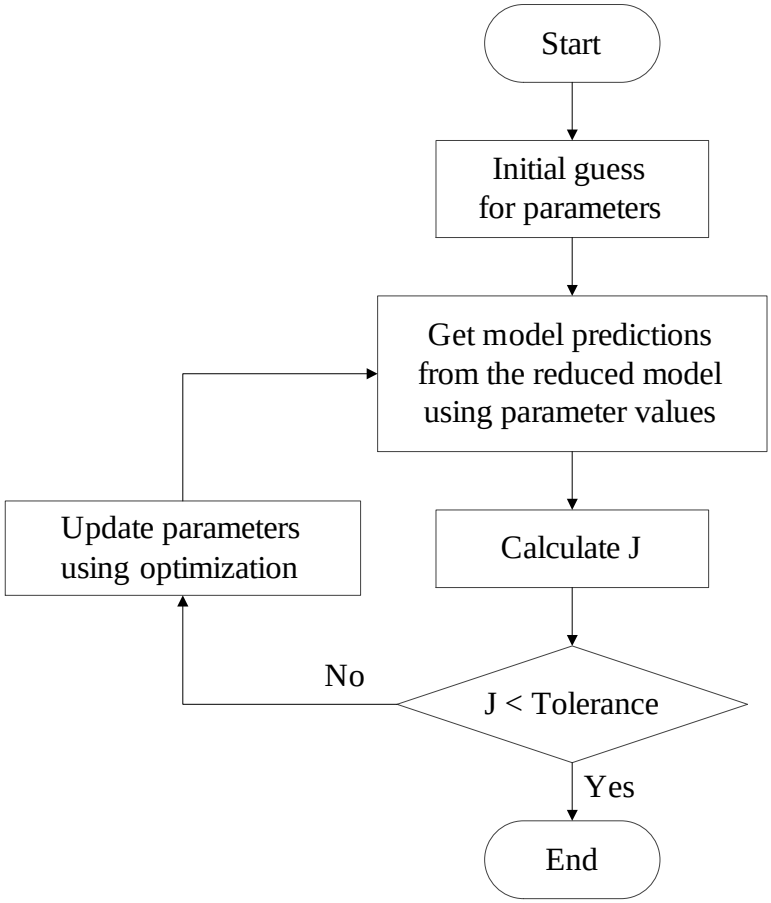

Figure 1.5: Estimation algorithm of measurement-based method

With the advent of phasor measurement unit (PMU), time-synchronized measurement data were used to obtain the modes and mode shapes of the inter-area oscillation [36] and a simplified model to represent inter-area interactions of large power networks was developed [37].

1.3 Dissertation Scope and Outline

The objective of this dissertation is to examine new methodologies that would alleviate the heavy computational demands for power-flow and transient stability analyses and achieve a high level of simulation accuracy. In order to fulfill the goal, nonlinear algebraic or dynamic equations are replaced with much simpler ones based on the power system criteria from engineering and mathematical perspectives. The proposed methods are roughly classified into two categories: complexity reduction in power-flow models corresponding to the algebraic equation set and simplification of the dynamic model equations. The power-flow model is modified by combining ac and dc models. The dynamic model reduction is done by removing highly negative eigenvalues. Overall methods for the dissertation are shown in Fig. 1.6.

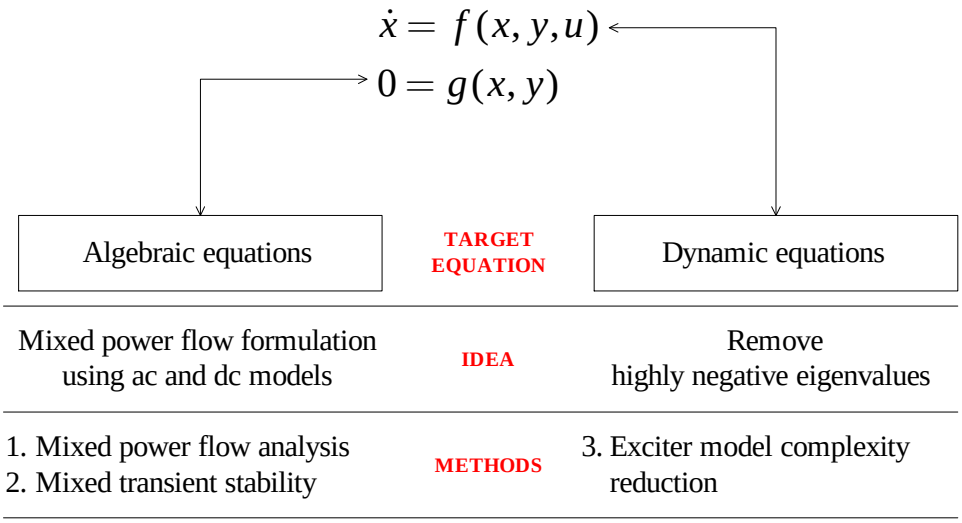

Figure 1.6: Scope of dissertation for computation time reduction

This dissertation contains three additional chapters. Chapter 2 presents a mixed approach using ac and dc models for power-flow analysis to decrease computational complexity and capture variations in the external system. A

high level of accuracy in the targeted central part of the system is achieved using the detailed ac model. The less detailed dc model is used to reduce computational requirements and still reflect changes in the external system. Chapter 2 starts with a brief analytic basis for power-flow analysis including ac and dc models. Then, the proposed approach is presented. The analytic calculations of computational benefits are provided. Case studies with the IEEE 118-bus system are presented to compare performance among the mixed approach, the ac and the dc models.

In Chapter 3, an advanced method for power system transient stability analysis is presented, allowing the reduction of the computational requirements while retaining important system dynamics. The mixed power-flow approach in Chapter 2 is extended to transient stability analysis. Chapter 3 first provides basics of power system transient stability simulation. Then, the mixed transient stability approach is proposed. To prevent the loss of simulation accuracy, how to compensate line losses neglected using the dc model is presented. The performance comparisons among the full model, the dynamic equivalent, and the proposed method are described with the IEEE 118-bus system.

Chapter 4 presents a condition-based exciter model reduction approach for improved transient stability simulation. Basic numerical integration methods are first explained. Conditions are investigated using practical power system examples when fast modes become active or inactive. Then, the proposed method is described, which switches dynamically between the original exciter model and the reduced one, depending on the switching criterion. Case studies with the GSO 37-bus and the Western Electricity Coordinating Council (WECC) system are provided to validate the performance of the proposed method.

Finally, concluding remarks are provided in Chapter 5. The promising topics for moving forward are also described.

CHAPTER 2

MIXED POWER FLOW ANALYSIS USING AC AND DC MODELS

2.1 Introduction

The function of an electric power system during normal operating conditions is to supply power to customers while maintaining voltage and frequency within predetermined limits. It is essential to know the voltages at each bus as well as the power flows through a transmission network in order to obtain complete understanding of the power system. Power flow analysis can provide this information, which can then be used to simulate the effectiveness of a future power system expansion plan. The simulation checks component overloading during peak load periods. Power flow analysis also allows system operators and planners to prepare for unpredictable contingency events such as loss of a generating unit or a transmission line outage. In addition, real-time results from periodically executed on-line power flow study are used to correct the power factor by compensating the reactive power and to allocate optimal generation to minimize transmission line losses and generation cost. Hence, power flow analysis is fundamental for operating and planning power systems.

The most accurate approach for power flow analysis is to model the electric power system with the classic power flow equations (ac model). The ac model is formulated by a set of nonlinear algebraic equations. An iterative algorithm is needed to solve it [38, 39]. Several problems are associated with

the ac model. The nonlinear equations may not converge when a good initial guess of the solution is not available [40]. High convergence reliability can be achieved with the time-consuming synthetic dynamics power flow method which adds artificial dynamic equations to the nonlinear equations [41]. The ac model is computationally expensive, especially when contingency analysis is considered.

A number of approximate models and different approaches to the power flow problem have been studied to improve performance. Some approximate models using physical properties of power systems, such as the decoupled and the dc power flow models, are the most commonly used analysis techniques in power systems [42, 43, 44]. These have faster solutions and simplicity. Examples include contingency analysis, transmission planning and market applications. Modifications for fast solution and less convergence difficulties of the decoupled model have been proposed [45, 46]. The quadratic power flow model provides faster convergence by using quadratic equations ideally suited to the Newton's method [47]. In addition, considering that uncertainty is always present in power systems, its incorporation into the solution process has been proposed [48, 49]. Either a probabilistic power flow or fuzzy power flow model is used, depending on how the uncertainty is expressed in the system.

Power systems have been required to operate more efficiently and economically since the deregulation of the power industry. To accomplish these objectives, it is important for power systems control centers to be able to analyze system states accurately and quickly. However, such analysis is a computationally demanding problem in large modern interconnected power systems, particularly for long-term simulations. To secure energy delivery systems, it is crucial to develop rapid and precise analysis methods in order

to have real-time situational awareness.

Many efforts have been made to speed up the power system analysis. Parallel computers using multiple processing units can achieve fast simulation without simplifying the transmission network [3]. Traditionally, network equivalent techniques have been used to reduce computational requirements [8]. Deckmann et al. give a comprehensive overview of classic methods to derive equivalent networks and their performance results in terms of accuracy, convergence and conditioning [11]. An analytic study based on practical experience and its application for security assessment can be found in [10, 50, 51]. Network equivalent techniques partition the electric network into the internal system, external system, and a group of boundary buses that divide the external system from the internal system. The size of the power network is reduced by eliminating the external system, while the internal system is unchanged. The effect of the external system on the internal one is included by adding real and reactive power flows to the boundary buses. In practical power systems, the internal system usually denotes the monitored part of the interconnected power system and is the area of interest of a regional utility.

However, it should be understood that the network equivalent approach is practical only for applications without variations in the external system or when knowledge of voltage states of the entire or the internal system is already available [9, 10]. This approach cannot capture changes in bus injections and network status of the external system because the external system was previously eliminated. As a result, the equivalent network needs to be updated whenever an alteration to the external system occurs. And the approach needs to have the solved power flow case for boundary matching: the net power flows between the unreduced and the reduced networks must be

an exact match in the boundary buses. Therefore, errors may be introduced when the solved power flow case is unknown.

This chapter presents an approach focused on reducing computational requirements for power flow studies, while being able to take into account bus injections and network status in the external system. The proposed method combines the ac and the dc power flow models. To achieve a high level of accuracy in the area of interest, power flow problems are formulated with the detailed ac model in the internal system. To reduce computational expense and reflect external variations, problems are solved with the less detailed dc model in the remaining system.

This chapter is organized as follows. Section 2.2 presents a brief analytic basis for power flow analysis. The proposed approach is presented in Section 2.3. Section 2.4 illustrates simulation results with the IEEE 118-bus system. A summary is presented in Section 2.5.

2.2 Power Flow Analysis

The basic formulation and solution of the power flow equations are presented briefly in this section.

2.2.1 AC power flow model

The formulation of the ac power flow equations begins with nodal analysis. The power balance equations are

$$P_k = V_k \sum_{m=1}^{N} V_m[G_{km}cos(\theta_k - \theta_m) + B_{km}sin(\theta_k - \theta_m)] \tag{2.1}$$

$$Q_k = V_k \sum_{m=1}^{N} V_m[G_{km}sin(\theta_k - \theta_m) - B_{km}cos(\theta_k - \theta_m)] \tag{2.2}$$

The real and reactive power balance equations in (2.1) and (2.2), respectively, are expressed with four variables: voltage magnitude, voltage phase angle, and net real and net reactive power injections. Two of the four variables at each bus are known, depending on the bus type. The remaining variables can be obtained by solving a set of nonlinear power balance equations. In order to solve for the unknowns in a power system, there must be the same number of equations as unknowns. The power balance equations at each bus are used. These equations can be formulated depending on the bus type.

- Load bus (PQ bus)

$$P_k^{sp} = V_k \sum_{m=1}^{N} V_m [G_{km} cos(\theta_k - \theta_m) + B_{km} sin(\theta_k - \theta_m)] \tag{2.3}$$

$$Q_k^{sp} = V_k \sum_{m=1}^{N} V_m [G_{km} sin(\theta_k - \theta_m) - B_{km} cos(\theta_k - \theta_m)] \tag{2.4}$$

- Generator bus (PV bus)

$$P_k^{sp} = V_k \sum_{m=1}^{N} V_m [G_{km} cos(\theta_k - \theta_m) + B_{km} sin(\theta_k - \theta_m)] \tag{2.5}$$

A resulting set of nonlinear equations can be solved with the Newton-Raphson (NR) method.

2.2.2 DC power flow model

The dc power flow model greatly simplifies the ac model with the following assumptions:

- Voltage magnitudes on all buses are 1 p.u.

- Voltage angle differences are small:
  $sin(\theta_k - \theta_m) \approx (\theta_k - \theta_m)$, $cos(\theta_k - \theta_m) \approx 1$
- Line resistance is negligible: $G_{km} \approx 0$
- Reactive power injections on all buses are ignored

Hence, the real power balance equation in (2.1) can be approximated as:

$$P_k = \sum_{m=1}^{N} B_{km}(\theta_k - \theta_m) \tag{2.6}$$

The dc model has computational advantages over the ac model. First, its equation set is just about half of the ac model, because it considers only the real power injections. Second, the dc model requires no iteration. Third, because the B matrix is independent of the states, only one factorization is necessary. Therefore, to find voltage states, the dc model is about ten times faster than the ac model [52]. Although the dc model is inherently approximate and may introduce error in power flow analysis, several previous attempts show that results using the dc model are reasonable and dc line power flows are, on average, offset by a few percentage points, as compared to the ac model [44, 53].

2.3 Proposed Method

The proposed approach formulates the power flow problem by combining the ac with the dc models in order to reduce the computational expenses and take the bus injections and network status in the external system into account. Power flow equations in the internal system, which require accurate solution, are formulated with the ac model and those in the external system are done

with the dc model for a faster but less detailed solution. Then, the reduced set of nonlinear equations is solved with the NR method. Figure 2.1 shows the procedure.

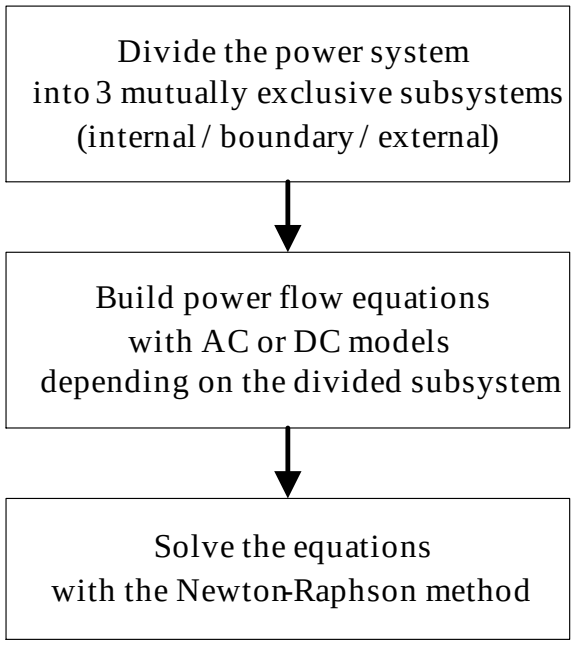

Figure 2.1: Procedure for the approach

2.3.1 Internal/external system and boundary buses

The power system can be divided into three mutually exclusive subsystems dependent on the area of interest which is called the *internal system*. The internal system is connected to neighboring systems, called the *external system*. A group of buses in the external system which have a connection with a bus in the internal system are called *boundary buses*. Figure 2.2 defines these three subsystems.

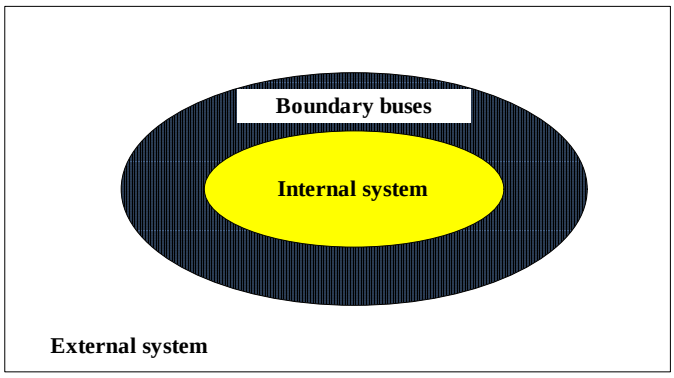

Figure 2.2: Schematic of internal system, boundary buses, and external system

2.3.2 Assumption of system information

It is assumed that all necessary information (net real and net reactive power injections for a PQ bus and net real power injection and voltage magnitude for a PV bus) is given in the internal system, whereas only net real power injection is given in the external system and at the boundary buses. Additionally, the complete network data is assumed to be known.

2.3.3 Boundary assumption

The effect of the external system on the internal system through the boundary buses should be considered in order to attain a high level of accuracy in the internal system. But the information given at the boundary bus is assumed to have only the net real power injection. Therefore, a proper guess for reactive power injection or voltage magnitude at the boundary buses is required. The voltage magnitude difference between two buses on a transmission line is usually around 1∼2%. Each boundary bus has at least one connection to the internal system bus whose voltage magnitude would be accurate because of a set of nonlinear equations with all given information. Thus, the best guess

for the boundary bus voltage magnitude would be to use that of the internal system. In addition, for a precise voltage phase-angle solution, nonlinear real power balance equations are built at the boundary buses. In other words, the approach assumes that the boundary buses are considered to be a PV bus with the voltage magnitude of a connected internal system bus without regard to bus type.

2.3.4 Power flow problem formulation

Depending on the subsystem, the power flow equations are formulated with ac or dc models as follows:

- Internal system
  - PQ bus: P, Q nonlinear equations using (2.3) and (2.4)
  - PV bus: P nonlinear equation using (2.5)
- Boundary buses
  - PQ/PV bus: P nonlinear equation using (2.3) with voltage magnitude of a connected internal system bus
- External system
  - PQ/PV bus: P linear equation using (2.6)

2.3.5 Power flow problem solution

The developed power flow problem is still a set of nonlinear equations, even though a set of linear equations is formulated in the external system. It can be solved with the NR method as follows.

- Build the Jacobian matrix

$$\underline{J} = \begin{bmatrix} \frac{\partial \underline{f}^p_{ext}}{\partial \underline{\theta}_{ext}} & \frac{\partial \underline{f}^p_{ext}}{\partial \underline{\theta}_{bd}} & 0 & 0 \\ \frac{\partial \underline{f}^p_{bd}}{\partial \underline{\theta}_{ext}} & \frac{\partial \underline{f}^p_{bd}}{\partial \underline{\theta}_{bd}} & \frac{\partial \underline{f}^p_{bd}}{\partial \underline{\theta}_{\text{int}}} & \frac{\partial \underline{f}^p_{bd}}{\partial \underline{V}_{\text{int}}} \\ 0 & \frac{\partial \underline{f}^p_{\text{int}}}{\partial \underline{\theta}_{bd}} & \frac{\partial \underline{f}^p_{\text{int}}}{\partial \underline{\theta}_{\text{int}}} & \frac{\partial \underline{f}^p_{\text{int}}}{\partial \underline{V}_{\text{int}}} \\ 0 & \frac{\partial \underline{f}^q_{\text{int}}}{\partial \underline{\theta}_{bd}} & \frac{\partial \underline{f}^q_{\text{int}}}{\partial \underline{\theta}_{\text{int}}} & \frac{\partial \underline{f}^q_{\text{int}}}{\partial \underline{V}_{\text{int}}} \end{bmatrix}$$

- The iterations are continued until the stopping criterion is satisfied

$$\underline{J}^{(i)} \begin{bmatrix} \Delta \underline{\theta}_{ext}{}^{(i)} \\ \Delta \underline{\theta}_{bd}{}^{(i)} \\ \Delta \underline{\theta}_{\text{int}}{}^{(i)} \\ \Delta \underline{V}_{\text{int}}{}^{(i)} \end{bmatrix} = - \begin{bmatrix} \underline{f}^p_{ext}(\underline{\theta}^{(i)}, \underline{V}^{(i)}) \\ \underline{f}^p_{bd}(\underline{\theta}^{(i)}, \underline{V}^{(i)}) \\ \underline{f}^p_{\text{int}}(\underline{\theta}^{(i)}, \underline{V}^{(i)}) \\ \underline{f}^q_{\text{int}}(\underline{\theta}^{(i)}, \underline{V}^{(i)}) \end{bmatrix}$$

$$\begin{bmatrix} \underline{\theta}_{ext}{}^{(i+1)} \\ \underline{\theta}_{bd}{}^{(i+1)} \\ \underline{\theta}_{\text{int}}{}^{(i+1)} \\ \underline{V}_{\text{int}}{}^{(i+1)} \end{bmatrix} = \begin{bmatrix} \underline{\theta}_{ext}{}^{(i)} \\ \underline{\theta}_{bd}{}^{(i)} \\ \underline{\theta}_{\text{int}}{}^{(i)} \\ \underline{V}_{\text{int}}{}^{(i)} \end{bmatrix} + \begin{bmatrix} \Delta \underline{\theta}_{ext}{}^{(i)} \\ \Delta \underline{\theta}_{bd}{}^{(i)} \\ \Delta \underline{\theta}_{\text{int}}{}^{(i)} \\ \Delta \underline{V}_{\text{int}}{}^{(i)} \end{bmatrix}$$

2.3.6 Example

When the simple power system in Fig. 2.3 is given and bus 1 is assumed to be a slack bus, the mixed approach can be applied as follows:

- System division

  If it is assumed that the internal system consists of buses 1, 2 and 3, the boundary buses, which have a connection to a bus in the internal one, are buses 4 and 5 and the remaining bus, 6, is the external system.

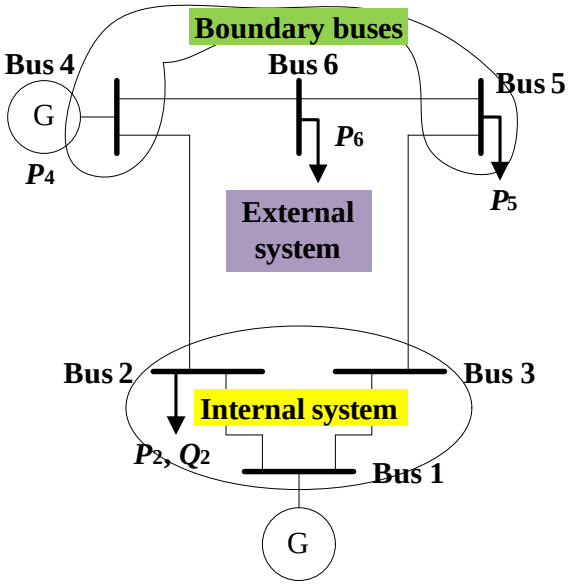

Figure 2.3: Six-bus system

- Formulate power flow equations
  - Internal system: P, Q nonlinear equations at buses 2 and 3

$$f_2^p = V_2 \sum_{m=1}^{N} V_m [G_{2m} \cos(\theta_2 - \theta_m) + B_{2m} \sin(\theta_2 - \theta_m)] + P_2 = 0$$

$$f_2^q = V_2 \sum_{m=1}^{N} V_m [G_{2m} \sin(\theta_2 - \theta_m) - B_{2m} \cos(\theta_2 - \theta_m)] + Q_2 = 0$$

$$f_3^p = V_3 \sum_{m=1}^{N} V_m [G_{3m} \cos(\theta_3 - \theta_m) + B_{3m} \sin(\theta_3 - \theta_m)] = 0$$

$$f_3^q = V_3 \sum_{m=1}^{N} V_m [G_{3m} \sin(\theta_3 - \theta_m) - B_{3m} \cos(\theta_3 - \theta_m)] = 0$$

– Boundary buses: P nonlinear equation at buses 4 and 5 with voltage magnitude of buses 2 and 3, respectively

$$f_4^p = V_2 \sum_{m=1}^{N} V_m[G_{4m}\cos(\theta_4 - \theta_m) + B_{4m}\sin(\theta_4 - \theta_m)] - P_4 = 0$$

$$f_5^p = V_3 \sum_{m=1}^{N} V_m[G_{5m}\cos(\theta_5 - \theta_m) + B_{5m}\sin(\theta_5 - \theta_m)] + P_5 = 0$$

– External system: P linear equation at bus 6

$$f_6^p = \sum_{m=1}^{N} B_{6m}(\theta_6 - \theta_m) - P_6 = 0$$

The total number of system unknowns with the mixed approach is seven, corresponding to the number of formulated equations. Therefore, the set of nonlinear and linear equations can be solved with the NR method. In contrast to the six-bus example, the dimensions of the external system in practical large-scale power systems are much larger than for the internal system, and thus compared to the set of nonlinear equations using the ac model alone, the reduced set of equations can be solved quickly.

2.3.7 Computational benefits

The proposed approach can reduce the computational requirements with the fast dc model in the external system. Estimation of the computational benefit from the mixed approach is explored by calculating the number of operations for LU factorization and forward/backward substitution requiring the solution of $\underline{A} \times \underline{x} = \underline{b}$, where A is the N × N nonsingular sparse matrix. According to [54], when each bus is assumed to have, on average, three branches, the computational complexity for LU factorization and forward/backward sub-

stitution for solving $\underline{A} \times \underline{x} = \underline{b}$ is assumed to grow as $N^{1.58}$ and $N^{1.29}$, respectively. The linearized matrix equation from the NR method at each iteration can be considered as $\underline{A} \times \underline{x} = \underline{b}$ and the dimension of the Jacobian matrix is linearly proportional to the number of equations which are formulated with power flow models.

To simplify the calculations, the number of operations is evaluated assuming that all buses except the slack bus are PQ bus and the number of boundary buses is small enough to be neglected. Most modern power flow code with the ac model treats the Jacobian as a matrix of 2 by 2 blocks. But, when the dc model is applied, the block is replaced with a 1 by 1 block. Therefore, the dc model is 8 times faster for the LU factorization and 4 times faster for the forward/backward substitution than the ac model. This allows the mixed approach to be faster. Table 2.1 shows the operations required for both the ac model and the mixed approach for any system having N buses with ratios of internal to external buses, e.g., 1:5 means that for every bus in the internal system, there are five in the external system. The computational benefits depend on the ratio. For the first iteration, the mixed approach is about 5 to 8 times faster for LU factorization and 3 to 4 times faster for forward/backward substitution than the ac model depending on the ratios of internal to external buses. The mixed approach can be even faster with the iteration of the NR method. It does not require updating the Jacobian elements related to the dc model because the B matrix of the dc model is constant. Therefore, computational benefits can be achieved by storing the elements obtained from the first iteration. The components of Jacobian matrix required to be updated are only for the ac model. When it is assumed that the NR method converges at the fourth iteration, the total number of operations with the mixed approach is 10 to 30 times smaller for LU fac-

torization and 6 to 15 times smaller for forward/backward substitution than with the ac model depending on the ratios of internal to external buses.

In addition, the use of the mixed approach allows us to neglect reactive power controls in the external system, such as LTC tap changing and generator PV-PQ switching. These controls usually require additional iterations for power flow solutions. The elimination of those issues can further increase the computational performance.

Table 2.1: Computational benefits from the mixed approach with N buses system

		The ration of internal to external buses			
		1:5		1:100	
		AC	Mixed	AC	Mixed
LU Factorization	Number of operations for the first iteration	[1/6*2*(N-1)]^1.58+ [5/6*2*(N-1)]^1.58 =2.42(N-1)^1.58	[1/6*2*(N-1)]^1.58+ 1/8*[5/6*2*(N-1)]^1.58 =0.46(N-1)^1.58	[1/101*2*(N-1)]^1.58+ [100/101*2*(N-1)]^1.58 =2.95(N-1)^1.58	[1/101*2*(N-1)]^1.58+ 1/8*[100/101*2*(N-1)]^1.58 =0.37(N-1)^1.58
	% of operation required	100%	19%	100%	12.5%
	Number of operations for the rest iteration	3*2.42(N-1)^1.58 =7.26(N-1)^1.58	3[1/6*2*(N-1)]^1.58 =0.53(N-1)^1.58	3*2.95(N-1)^1.58 =8.85(N-1)^1.58	3*[1/101*2(N-1)]^1.58 =0.006(N-1)^1.58
	Total	9.68(N-1)^1.58	0.99(N-1)^1.58	11.8(N-1)^1.58	0.38(N-1)^1.58
	% of operation required	100%	10.2%	100%	3.2%
Forward and Backward Substitution	Number of operations for the first iteration	[1/6*2*(N-1)]^1.29+ [5/6*2*(N-1)]^1.29 =2.18(N-1)^1.29	[1/6*2*(N-1)]^1.29+ 1/4*[5/6*2*(N-1)]^1.29 =0.73(N-1)^1.29	[1/101*2*(N-1)]^1.29+ [100/101*2*(N-1)]^1.29 =2.42(N-1)^1.29	[1/101*2*(N-1)]^1.29+ 1/4*[100/101*2*(N-1)]^1.29 =0.61(N-1)^1.29
	% of operation required	100%	33.5%	100%	25.2%
	Number of operations for the rest iteration	3*2.18(N-1)^1.29 =6.54(N-1)^1.29	3*[1/6*2*(N-1)]^1.29 =0.73(N-1)^1.29	3*2.42*(N-1)^1.29 =7.26(N-1)^1.29	3*[1/101*2*(N-1)]^1.29 =0.02(N-1)^1.29
	Total	8.72(N-1)^1.29	1.46(N-1)^1.29	9.68(N-1)^1.29	0.63(N-1)^1.29
	% of operation required	100%	16.7%	100%	6.5%

2.4 Case Study

Case studies were performed with the IEEE 118-bus system [55]. For the purpose of investigation, three simulations were conducted by changing the internal system as shown in Fig. 2.4. If the internal system for Test 1 is chosen for simulation, then everything else would be either the external system or the boundary buses. Details of this division of the IEEE 118-bus system for three simulations are also provided in Table 2.2.

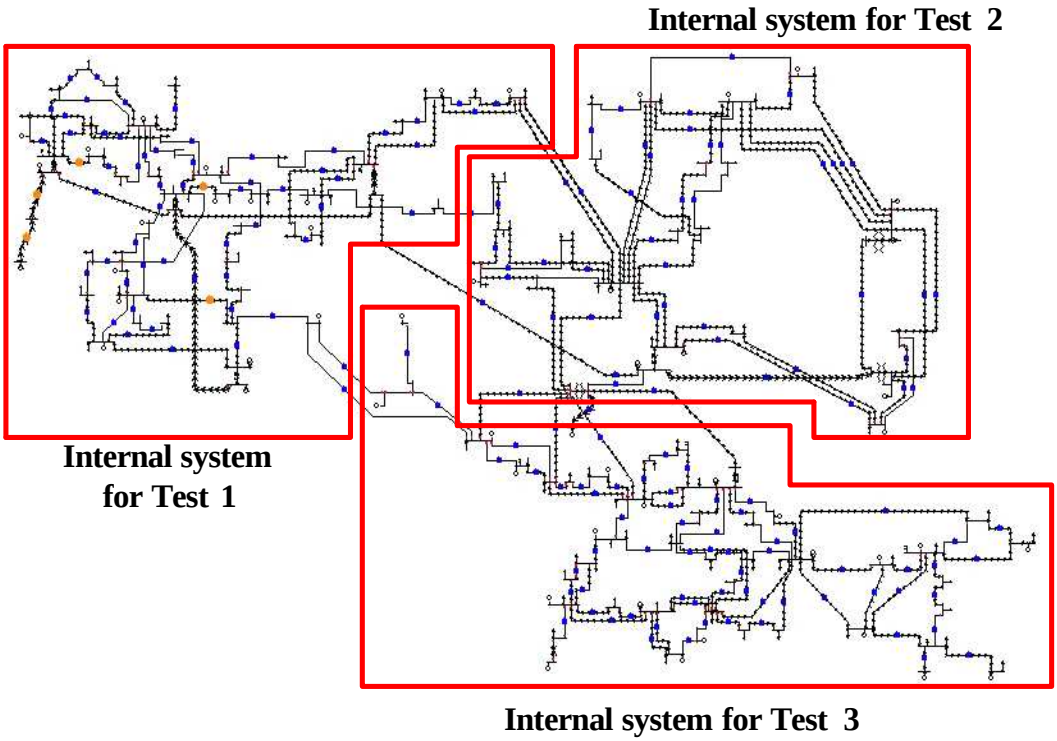

Figure 2.4: Three internal systems selected for simulation with the IEEE 118-bus system

Table 2.2: Details of the division for three simulations

	Internal system buses	Boundary buses
Test 1	1∼43, 113∼115, 117 (47 buses)	44, 49, 65, 70, 72
Test 2	44∼68, 116 (26 buses)	38, 42, 43, 81
Test 3	70∼112, 118 (44 buses)	24, 68

Errors are evaluated by comparing the states using the ac model in the whole system with those using the mixed approach. In addition, errors from the dc model are also computed to compare it with the proposed approach. The Euclidean norm of the errors (2.7) and a sum of the Euclidean norm of the errors (2.8) in the internal system are commonly used for state estimation [56]. They combine both voltage-magnitude and voltage phase-angle errors.

$$EN_i = \left\| \overline{V_{i(AC)}} - \overline{V_{i(estimate)}} \right\| \tag{2.7}$$

$$\text{Sum of EN} = \sum_{i \in internal} \left\| \overline{V_{i(AC)}} - \overline{V_{i(estimate)}} \right\| \tag{2.8}$$

Simulation results are provided in Fig. 2.5 and Table 2.3. The figures show the Euclidean norm of the error at each bus. The error in the selected internal system is small and it means that the states obtained from the mixed approach in the internal system are reasonably close to those using the ac model.

Table 2.3: Sum of Euclidean norm from three simulations

	Mixed approach (A)	DC model (B)	Error rate of mixed approach compared to DC model (=A/B×100%)
Test 1	0.0236	2.8853	0.82%
Test 2	0.0269	0.9215	2.92%
Test 3	0.0713	1.4502	4.92%

In Table 2.3, the sum of the Euclidean norm of the all bus errors in the internal system is calculated. The results from the mixed approach are compared to those from the dc model. The sum of the errors in the internal system from the mixed approach is small compared to the dc model. The error value is dependent on the test cases. The boundary assumptions for the mixed approach may introduce different amounts of errors depending on

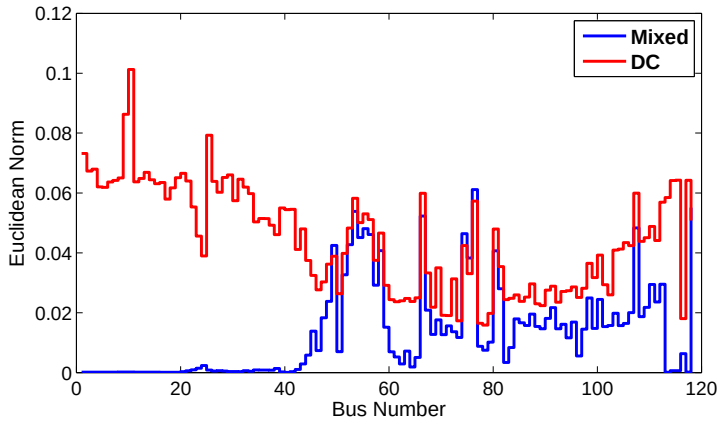

(a) Test 1 (Internal system: from bus 1 to 43 and 113, 114, 115, 117)

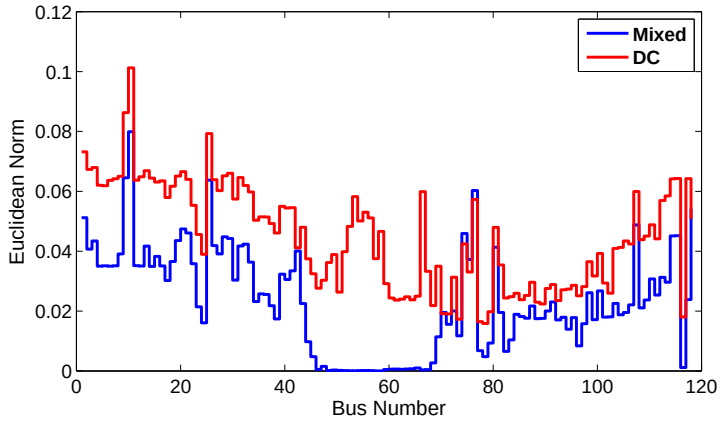

(b) Test 2 (Internal system: from bus 44 to 68 and 116)

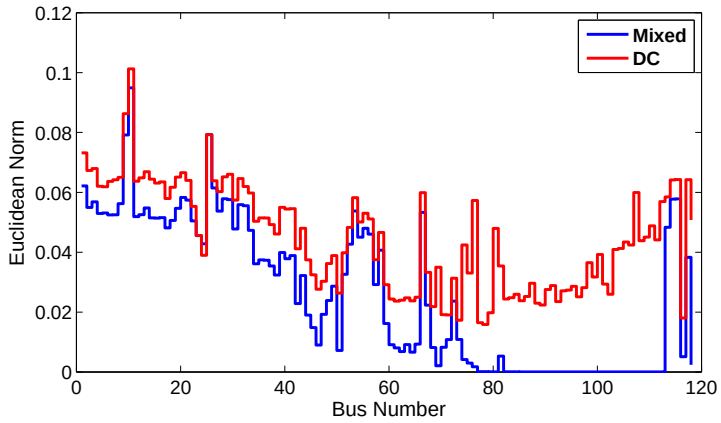

(c) Test 3 (Internal system: from bus 70 to 112 and 118)

Figure 2.5: Simulation results with the IEEE 118-bus case

the simulation cases.

Table 2.4 shows the computation time of three test cases and the results from the mixed approach are compared to that from the ac model. All cases are converged at the fourth iteration. The simulation time is dependent on the case study having a different ratio of internal to external buses. More speed benefits can be achieved with a higher ratio in practical larger power systems.

Table 2.4: Computation time of three case studies

	AC model	Mixed approach		
		Test 1	Test 2	Test 3
Ratio of internal to external buses	-	1:1.4	1:3.3	1:1.6
Computation time [sec]	1.37	0.74	0.56	0.65
% of time	100%	54%	41%	47%

2.5 Summary

This chapter explores the development of power flow algorithms for combining the detailed ac model with the less detailed dc model. The approach gives an advanced power flow model which has a fast solution, about ten–thirty times for LU factorization and six–fifteen times for forward and backward substitution faster than using the ac model alone, without sacrificing accuracy in areas of interest. It can be used for any size of power system. More benefits in terms of speed can be achieved with a larger power system case and higher dimension of the external system compared to the internal system. The approach also includes the external system, in contrast to the network equivalent technique. This approach can be utilized in a variety of power system applications.

CHAPTER 3

MIXED TRANSIENT STABILITY ANALYSIS USING AC AND DC MODELS

3.1 Introduction

With power systems being operated closer to their security limits, it is critically important that utilities have access to powerful computation tools that can perform rigorous analysis of transient behavior [57]. However, due to interconnections, modern power grids have become increasingly complex. They are comprised of millions of loads and generators, and tied together by hundreds of thousands of miles of transmission and distribution wires with a myriad of control devices. As a result, a power system transient stability simulation for dynamic security assessment is required to solve a huge number of nonlinear differential algebraic equations (DAE) and needs to be run for many contingency cases [2]. Computational demands in terms of storage and simulation time are significant. For many decades, it has been an open challenge to achieve fast and accurate power system transient stability analysis.

Traditionally, dynamic equivalents have been used to reduce the computational burden. This approach retains an area of interest for study, called the *internal system* and replaces the *external system* — neighboring areas connected to the internal system — with an electrical equivalent. The power system model is thus reduced in size. There are three general approaches used to develop these equivalents: *modal*, *coherency* and *measurement-based*

[18, 28]. While certainly useful in some situations, the equivalent approach has weaknesses in that the equivalent must be updated whenever the operating point or system topology is substantially changed [31] and the simulation accuracy of the traditional equivalent methods is dependent on the type of disturbance (fault) [58].

One example of a disturbance that can usually be addressed quite well by the use of a substantially reduced equivalent is a bus fault and subsequent line opening actions. The effects will be associated mostly with the nearby voltage magnitudes. The frequency impact is small because such disturbances do not usually create a substantial imbalance between the electric load and generation. The reduced system with the buffer zone around the fault and with an appropriate dynamic equivalent at the boundary buses can give accurate responses [18, 28, 31, 58].

On the other hand, when generator or load outages happen, the situation is different in that the frequency perturbation will affect the entire power system. The use of the traditional equivalent could be inappropriate to represent system responses correctly. One issue would be if the dynamic equivalent does not have enough reserve generator governor response to make up for the generator loss or the load increase. The reduced system cannot maintain additional real power injections from the already removed external system. Therefore, an enhanced transient stability simulation method is required both to reduce the computational requirements and to achieve better simulation accuracy than the pure equivalent approach.

Chapter 2 presented a hybrid power flow approach that combines full ac models with a less detailed dc power flow models. Here the approach is extended to transient stability analysis. The idea originates from the fact that although reactive power does not travel well in power systems because

the transmission network is mostly inductive, the real power does. Both real and reactive power dynamics are dominant in the internal system where any type of fault occurs. For the external system which is impacted by a fault in the internal system, real power dynamics play a more important role. The significant dynamics of both areas can be preserved by formulating different power flow equations at each region. The detailed ac model, including full real and reactive power equations, is used for the area of interest, while the simpler dc model, including only linear real power equations, is used for more remote areas. In order to prevent the loss of simulation accuracy, this approach presents a way to compensate for the line losses neglected using the dc model. Therefore, the approach can reduce the computational requirements, and still achieve a high level of simulation accuracy in the area of interest.

This chapter is organized as follows. Section 3.2 presents a brief analytic basis for the power system transient simulation and power flow models. The proposed approach is presented in Section 3.3. Section 3.4 illustrates simulation results with the IEEE 118-bus system. A summary is presented in Section 3.5.

3.2 Power System Transient Simulation

3.2.1 Transient stability simulation

A transient stability simulation involves solving a set of differential equations and an accompanying set of algebraic equations shown in (3.1) and (3.2) [59, 60]. These are called differential algebraic equations and are of the

following forms:

$$\dot{x} = f(x, y) \tag{3.1}$$

$$0 = g(x, y) \tag{3.2}$$

Equation (3.1) represents the power system dynamics, with the x variables showing the dynamic state variables such as generator rotor angles and speed. The dimension of vector x is dependent on the modeling detail and the size of the power systems. Equation (3.2) represents the stator and network algebraic equations, with the y variables showing algebraic variables such as the network bus voltage and angles. The dimension of vector y equals twice the number of buses.

Figure 3.1 shows a flowchart of a typical transient program which solves the above set of mathematical equations. The first step is to find the initial conditions. Those values are determined from power flow solutions and by setting all the differential operators to zero. Then the time-domain solutions of the equation sets are obtained through either explicit or implicit numerical integration formulas applied to each differential operator. This gives a set of algebraic equations which is then solved by an iterative method, such as the Newton method. When a disturbance occurs at a certain time, dynamic or algebraic equations are changed accordingly. This process repeats until the simulation time reaches its end time.

3.2.2 AC power flow model

In the ac model approach, the power balance equations are represented by the equations (3.3) and (3.4). These are associated with the algebraic equation (3.2) for transient stability analysis.

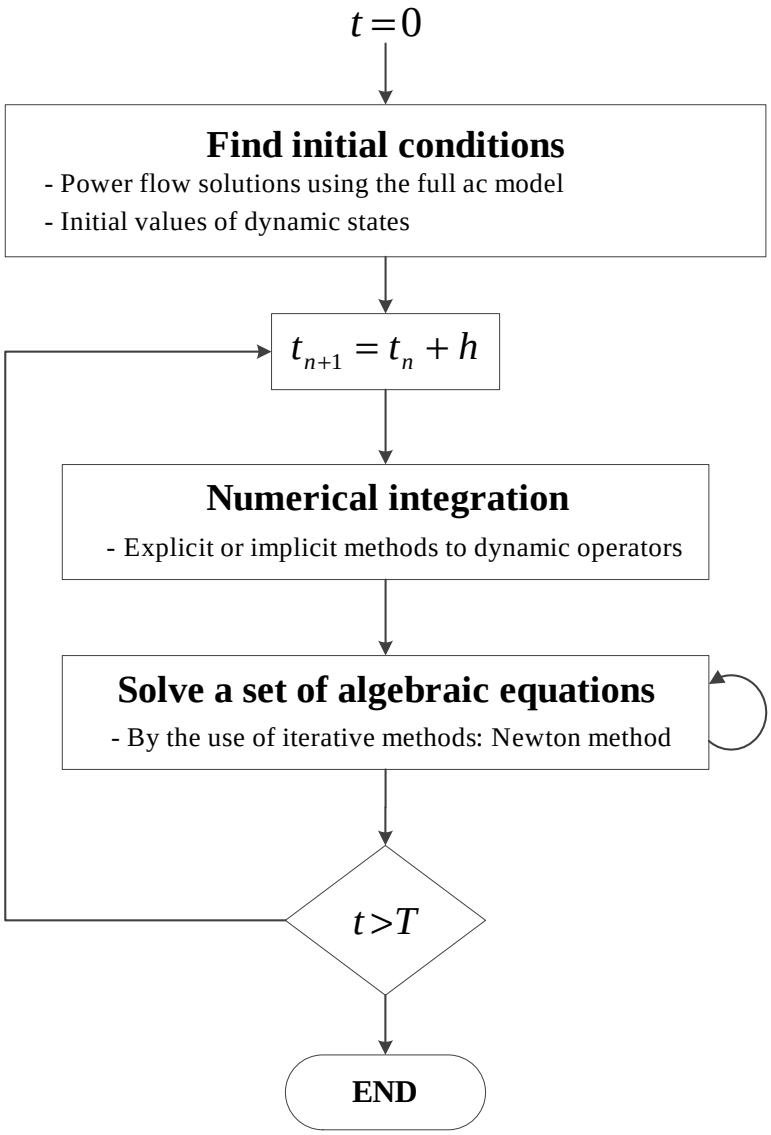

Figure 3.1: A flowchart of a conventional transient simulation

$$P_k = V_k \sum_{m=1}^{N} V_m[G_{km}cos(\theta_k - \theta_m) + B_{km}sin(\theta_k - \theta_m)] \tag{3.3}$$

$$Q_k = V_k \sum_{m=1}^{N} V_m[G_{km}sin(\theta_k - \theta_m) - B_{km}cos(\theta_k - \theta_m)] \tag{3.4}$$

The ac model is formulated with nonlinear equations. An iterative algorithm is required to solve those equations. Thus the ac model is computationally expensive, especially for transient stability analysis which must find a solution for every time step.

3.2.3 DC power flow model

The dc model simplifies the ac model by making several assumptions. These are (1) the reactive power balance equations are completely ignored, (2) all voltage magnitudes are one per-unit, (3) voltage angle differences are small enough, and (4) line losses are ignored. Hence the dc model reduces the size of the power flow problem and changes nonlinear problems to a set of linear equations. It is represented with the following equation:

$$P_k = \sum_{m=1}^{N} B_{km}(\theta_k - \theta_m) \tag{3.5}$$

Even though the assumptions reduce simulation accuracy, the dc model has been widely used because of its computational advantages over the ac model. It can run many times faster because of the following reasons. The dc model reduces the size of the equation set to about half of the ac model, because the reactive power equations are ignored. The model is linear. Thus

no iterations are required and only one factorization of the B matrix is needed no matter what operation conditions are considered.

3.3 Proposed Method

The proposed method formulates the algebraic equations for transient stability simulation by combining the ac with the dc power flow models, depending on the area of interest. The detailed ac model is used for the internal system where both real and reactive power dynamics are dominant. The simpler dc model is used for the external system where real power dynamics dominate. The proposed method can then represent both the localized effects related to real and reactive power flows using the ac model for the internal system, and the entire effects mostly related to real power flows using the dc model for the external system. Thus, the proposed method aims to achieve a high level of simulation accuracy with the full ac model in the internal system and to speed up transient stability simulation with the linearized dc model.

3.3.1 Boundary bus modeling

In the proposed approach, the more approximate dc model is used in the external system. The external system makes an impact on the internal system through the boundary buses that comprise the boundary between the two systems. Careful considerations should be made at the boundary buses to minimize the error propagation from the external system. A high level of accuracy can then be achieved in the internal system where accurate solutions are required. Thus, the more accurate ac model is used to formulate the algebraic equations at the boundary buses.

3.3.2 Loss compensation in the external system

The dc model applied to the external system does not take into account the losses, which have the potential to introduce a usually relatively small error in the branch MW flows. However, for larger power systems the cumulative sum of these individually small errors might not be negligible and total real power balances might not be preserved [44]. Therefore, the dc model cannot capture the widespread real power impact accurately from the internal system. The proposed approach expects that the dimension of the external system would be much larger than the internal system. It is thus necessary to compensate for these losses to maintain the real power balances in the external system. The proposed approach converts the losses into shunt resistances at each external bus. The loss can be obtained from (3.3) and has the following form:

$$P_{loss(k)} = V_k \sum_{m=1}^{N} V_m [G_{km} cos(\theta_k - \theta_m)] \tag{3.6}$$

The loss modeling is based on the initial ac power flow solution and it is performed before the transient simulation loop. The power balance equations for the external system have the following form:

$$P_{k(external)} = \sum_{m=1}^{N} B_{km}(\theta_k - \theta_m) + P_{loss(k)} \tag{3.7}$$

3.3.3 Proposed approach

In the proposed method, the set of algebraic equations corresponding to the system network can be summarized as follows:

- Internal system and boundary buses
  - Nonlinear P and Q equations using (3.3) and (3.4)
- External system
  - Linear P equation with loss addition using (3.7)

Figure 3.2 shows a flowchart of the proposed transient stability approach. Compared to the conventional method, most of the procedures are the same, but the presented approach adds the loss modeling for the external system and formulates new power flow equations, depending on the area of interest.

3.3.4 Computational benefits

As shown in Figs. 3.1 and 3.2, transient simulations need to solve a set of algebraic equations for every time step. The use of the dc model in the external system reduces the dimension of the equations and thus the computational requirements can be reduced greatly. The benefits are dependent on the ratio of the number of internal buses to external buses. More computational reductions can be achieved when the dc area is much larger than the ac area. Analytic details about computational benefits depending on the ratio are shown in Chapter 2. In addition, the dc model does not consider voltage magnitude variation and reactive power-flows, such that dynamic equations associated with them can be removed in the external system. Those dynamics usually show very fast dynamics. Therefore, additional speedup can be made

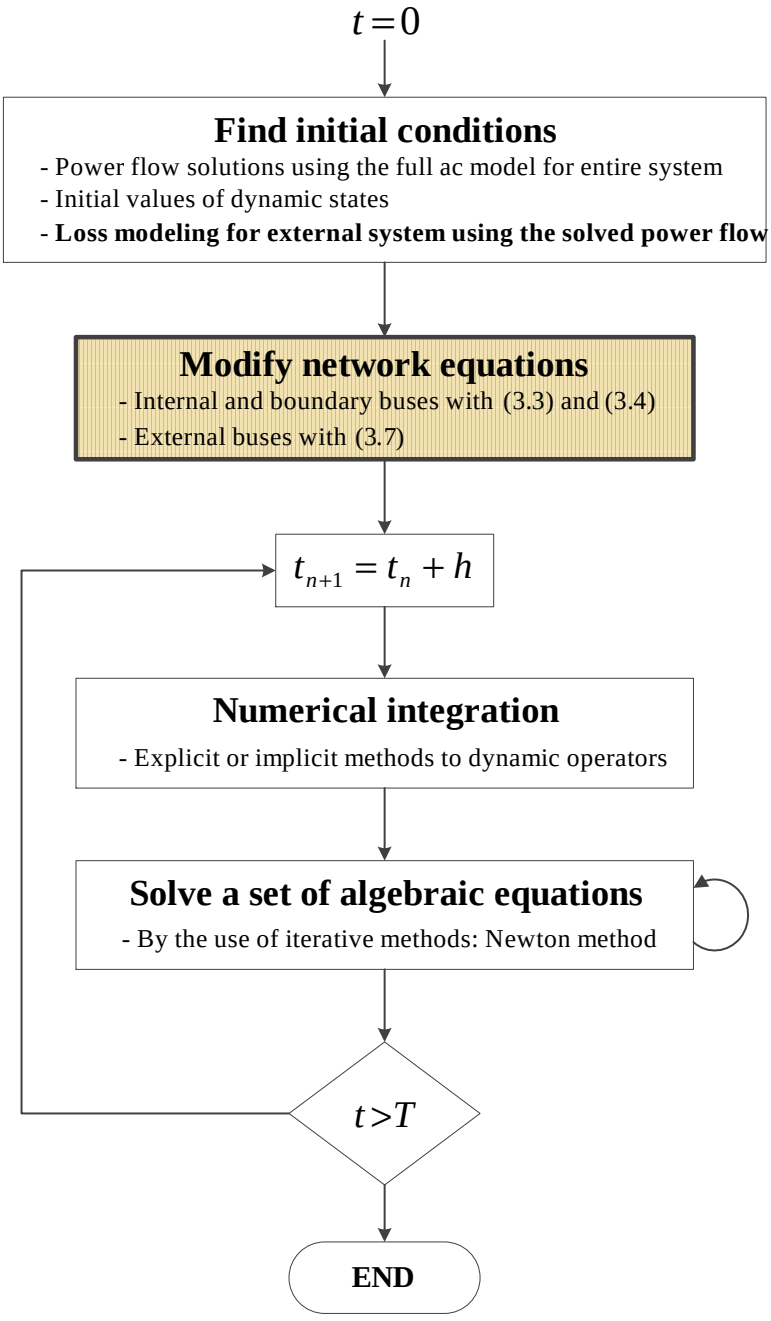

Figure 3.2: A flowchart of the proposed transient stability analysis

by neglecting the dynamic equations associated with the voltage magnitude and the reactive power flow, and by using a larger numerical integration time step in the external system without numerical instability issues.

3.4 Case Study

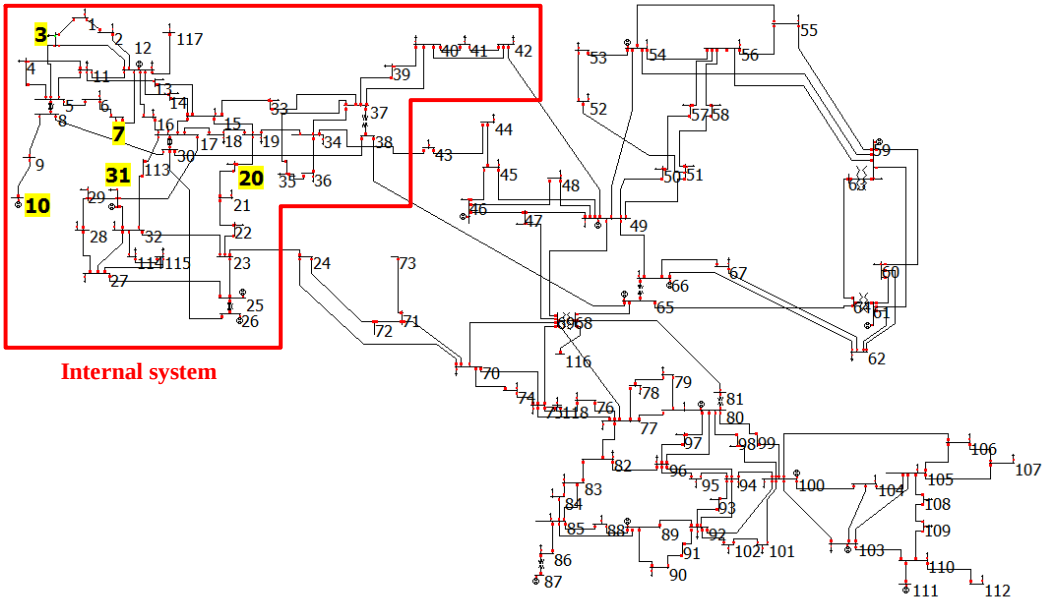

Figure 3.3: One-line diagram of the IEEE 118-bus system

The proposed approach is implemented with Matlab. The performance of the proposed method is validated with the IEEE 118-bus system shown in Fig. 3.3 [55]. The case contains 186 branches, 19 generators and 99 loads. System dynamics are represented with the classical machine model in equation (3.8) [61] and the simple TGOV1 (turbine-governor) model of which block diagram is depicted in Fig. 3.4 [62]. Constant impedance loads are modeled. Detailed model parameters for simulations are presented in Appendix A.1.

$$\frac{d\delta_i}{dt} = \omega_i - \omega_s \tag{3.8a}$$

$$\frac{2H_i}{\omega_s}\frac{d\omega_i}{dt} = T_{Mi} - T_{Ei} - D_i(\omega_i - \omega_s) \tag{3.8b}$$

where

δ_i : Rotor angle position of machine i

ω_i : Rotor angle velocity of machine i

H_i : Inertia constant of machine i

T_{Mi} : Mechanical torque of machine i

T_{Ei} : Electrical torque of machine i

D_i : Damping coefficient of machine i

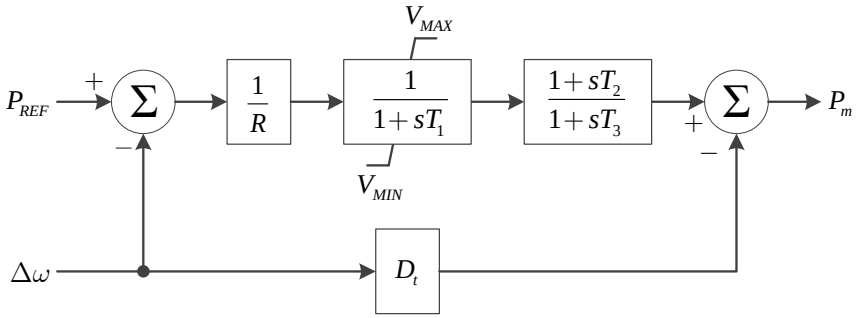

Figure 3.4: Block diagram of TGOV1

Table 3.1: Details of the system division

	Buses
Internal system	1∼23, 25∼42, 113∼115, 117 (45 buses)
Boundary buses	24, 43, 49, 65

The mixed transient method is tested with the system division provided in Table 3.1. Overall there are 45 buses in the internal system, four boundary buses, and 69 buses in the external system. In this example, two different types of disturbance are applied: (1) a load addition to cause a systemwide frequency variation, and (2) a balanced three-phase bus fault to ground to examine a more localized disturbance. The steady-state operating points are then disturbed and dynamic responses are compared.

Simulation comparisons are made between the full system model, a standard equivalent model, and the proposed mixed ac-dc approach. A dynamic equivalent circuit including dynamic parameters is obtained from PowerWorld simulator [63]. The difference is measured using RMSE (Root Mean Square Error) over the simulation period [64].

$$RMSE = \sqrt{\frac{1}{N}\sum_{i=1}^{N}(x_{full-model} - x_{estimate})^2} \tag{3.9}$$

where N is the number of simulation time steps and x is time-series data compared.

3.4.1 Load addition (100 MW) at bus 3

For the first disturbance, the load (100 MW) at bus 3 is off-line initially and is changed to on-line at 0.1 sec. The load connection introduces real power imbalance in the system and the individual generators via governor control supply additional real power to restore the system frequency.

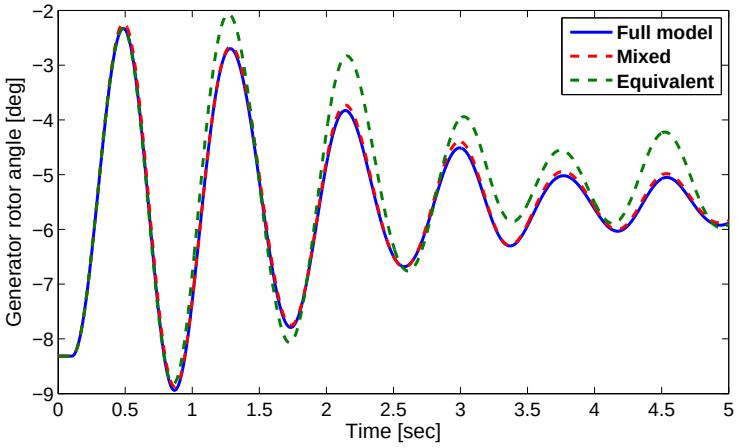

Figure 3.5: Relative rotor angle of Generator 31 w.r.t. Generator 12

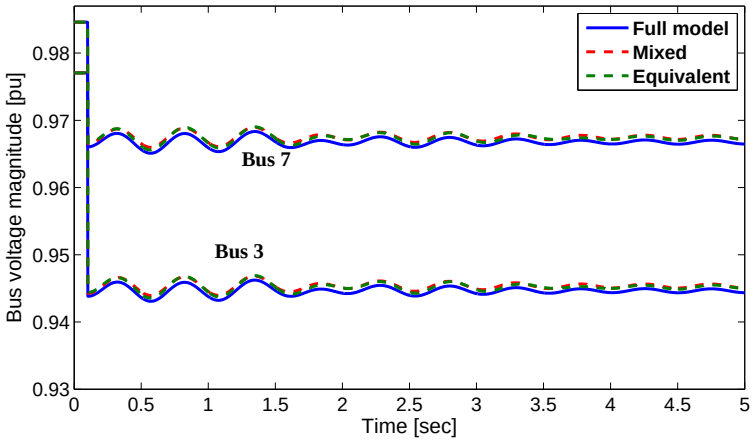

Figure 3.6: Simulation comparisons of bus voltage magnitude

Figure 3.5 shows the relative rotor angle of Generator 31 with respect to Generator 12, and the bus voltage magnitudes for the internal system are presented in Fig. 3.6. The responses from the proposed method show overall good agreement with those from the full transient stability approach. The RMSE in (3.9) over the period from 0 to 5 seconds is shown in Figs. 3.7 and 3.8. The reduced system from the equivalent method does not produce simulation results in the external area and thus the RMSE for the external buses are expressed with zero.

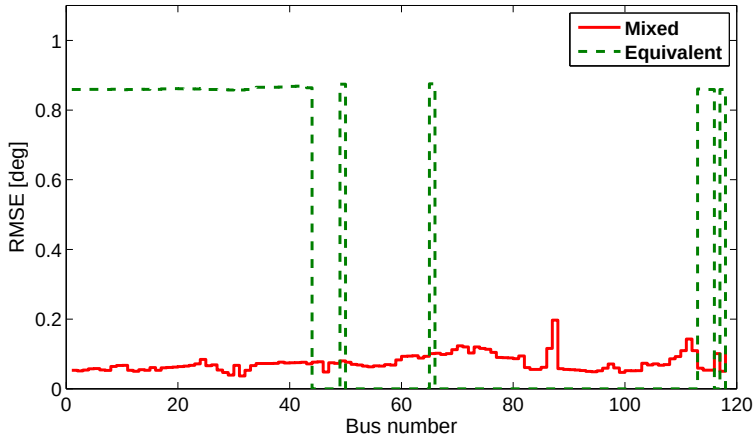

Figure 3.7: RMSE of bus voltage angle

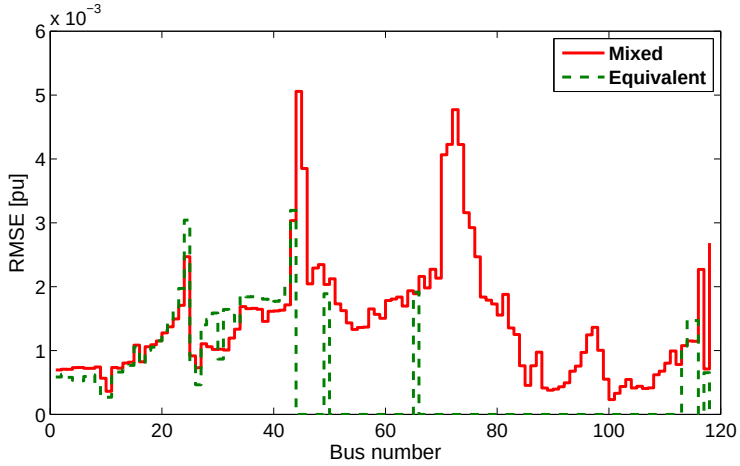

Figure 3.8: RMSE of bus voltage magnitude

As shown in the Fig. 3.7, the mixed method shows a smaller RMSE compared to the dynamic equivalent and it means that the proposed method provides better matching with the full model method than the dynamic equivalent. And the angle differences in the external system from the mixed method are similar with those in the internal system. It can be understood that the dc model shows a quite good performance to represent the real power dynamics.

3.4.2 Bus to ground fault at bus 3

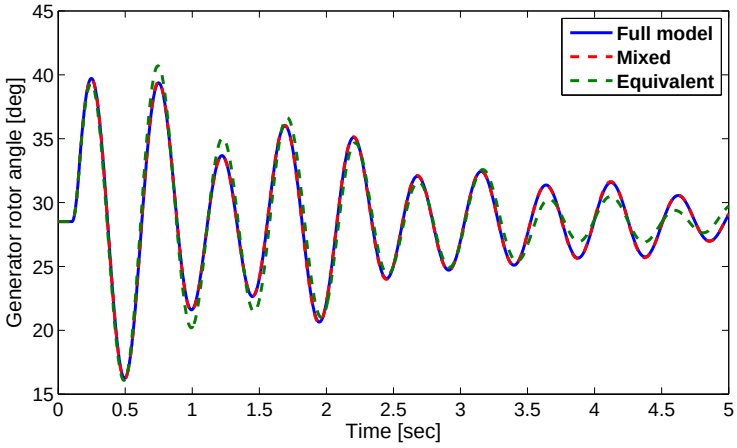

Figure 3.9: Relative rotor angle of Generator 10 w.r.t. Generator 12

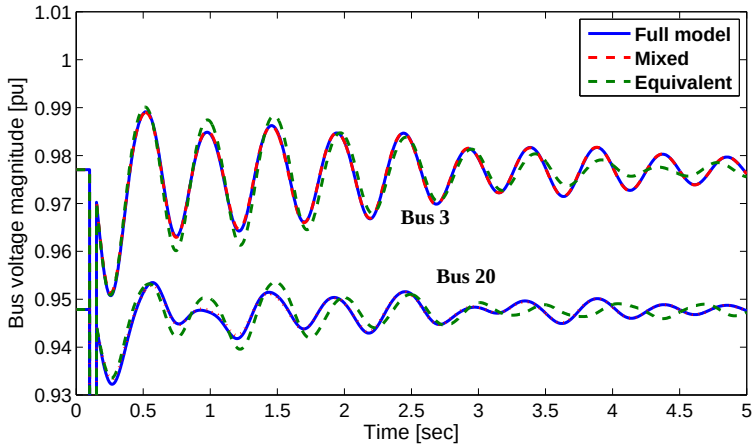

Figure 3.10: Simulation comparisons of bus voltage magnitude

The second comparison is with the simulation of a bus to ground fault. A three-phase bus to ground fault is applied at bus 3 at 0.1 second and cleared at 0.15 second. Unlike the previous load connection, the fault does not introduce any significant real power imbalance between the net generation and load, causing real and reactive power variations mostly in the buses close to the fault location. Figures 3.9 and 3.10 show the simulation comparisons with Generator 10's rotor angle and bus voltage magnitudes, respectively.

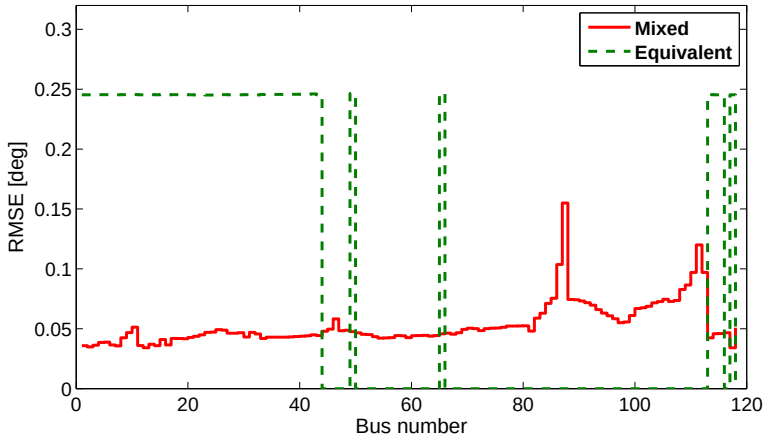

Figure 3.11: RMSE of bus voltage angle

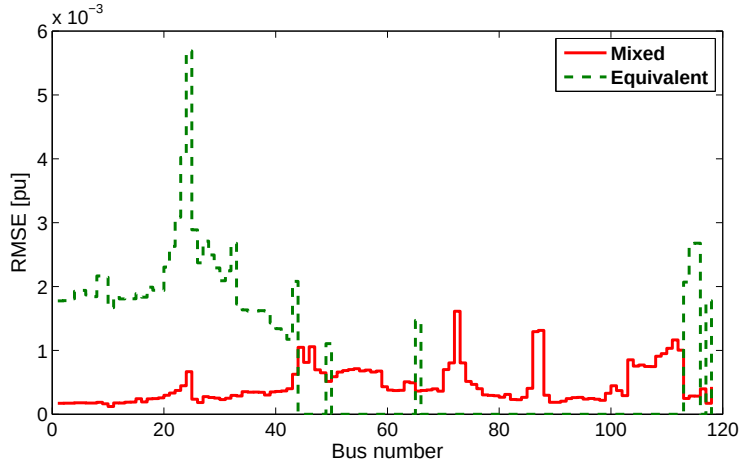

Figure 3.12: RMSE of bus voltage magnitude

With the bus to ground fault, the proposed method shows virtually identical responses to the full model method. The fault makes an impact locally, mostly on the internal system. This is because the impact of the bus to ground fault is dependent on the electrical distance between the bus fault location and the neighboring buses. When the fault occurs far from a bus, its impact on the bus is lessened. Therefore, the deviation of the system states in the external system is very small and the use of the more approximate dc model does not introduce a big difference in the internal system.

Furthermore, as shown in Fig. 3.12, the voltage magnitude errors in the external system are quite small even though the proposed method deals with the fixed voltage magnitude. As shown in Figs. 3.11 and 3.12, the simulation results of both angle and voltage magnitude validate that the proposed method accomplishes better accuracy than the dynamic equivalent method.

3.4.3 Computational benefits and accuracy

The computation time with different simulation approaches and the 118-bus system is provided in Table 3.2. The equivalent method gives a faster solution than the proposed method. However, additional computational time is needed to obtain the equivalent and this is not included in the time computation. In addition, a new equivalent must be reevaluated whenever operating point or system topology is altered. The mixed approach needs no extra time. For the given system configuration, the ratio of the internal to external buses is about 1 to 1.4. More computational benefits can be attained with the case where the external system is much bigger than the internal system.

Table 3.2: Computation time of 118-bus case

Method Used	Ratio of Computation Time
Full Model	1
Mixed	0.73
Equivalent	0.39

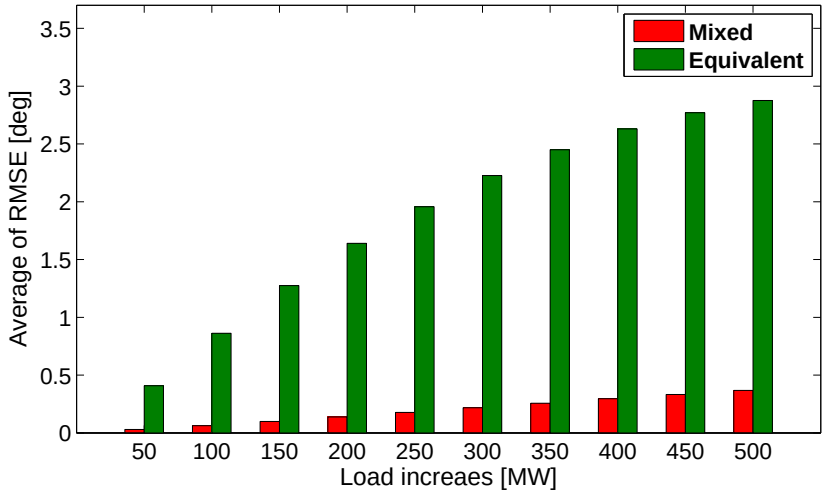

Figure 3.13: Average of bus angle RMSE with varying load amount at bus 3

Figure 3.13 shows accuracy comparison between the mixed and the equivalent methods when the amount of the load addition at the bus 3 is varied from 50 MW to 500 MW. The average of RMSE angle values for the buses in the internal system is computed. The equivalent approach shows bigger discrepancy in responses as the load amount increases. Conversely, the mixed approach provides quite good accuracy whatever load amounts are added. Because the equivalent system does not maintain the generators in the external area, additional injections from those generators cannot be obtained with the equivalent approach.

3.5 Summary

An alternative method that speeds up transient stability simulations while still maintaining a high level of simulation accuracy has been proposed. It is based on the fact that the reactive powers tend to be more localized compared to real powers. In the area of interest, where the disturbances are applied and accurate simulation outcomes are required, both real and reactive power

equations should be considered to represent power system dynamics correctly, while real power equations would be enough in the more remote areas where real power dynamics are dominant. The proposed approach thus formulates power flow equations for transient stability simulation by combining the full ac and dc models. A detailed ac model, including nonlinear real and reactive power equations, is used in the internal system, while a simpler dc model is used in the external system. The real power losses ignored by the standard dc model are compensated for in the external system by using the initial power flow solutions. The test simulations performed with the IEEE 118-bus system have confirmed that the proposed method achieves faster and accurate solutions. It is expected that the proposed method would be a promising solution for the advanced study of transient stability.

CHAPTER 4

EXCITER MODEL COMPLEXITY REDUCTION FOR IMPROVED TRANSIENT STABILITY SIMULATION

4.1 Introduction

Faster transient stability simulations can be achieved by considering the power system dynamic characteristics and the numerical integration method. Power system dynamics often involve a wide variety of different time frames even just within the transient stability problem [61]. Some widely used commercial transient stability packages employ explicit numerical integration methods, and others use implicit methods. When solving ordinary differential equations (ODEs) with varying time scales, explicit numerical integration methods require relatively small time steps to avoid numerical instability. In practical power systems, only a small fraction of system states are associated with the faster dynamics. Thus, it would be inefficient to simulate the entire system with the required small time step.

A common technique used in explicit transient stability packages to avoid this computational issue is through the use of multirate methods, in which different variables are integrated with different time steps [65]. Such an approach uses small time steps for fast varying variables and larger time steps for the slowly varying ones. The equations for the fast-changing variables must be solved at points where the slower ones are not solved. In these equations, linear interpolated values are used for the slow variables. For a large power system with very few fast variables, the multirate method can

provide immense computational benefits. This approach was first applied to the power system transient stability problem in [66] and advanced in [67, 68].

An example of a practical stiff power system is the Western Electricity Coordinating Council (WECC) system. The single machine infinite bus (SMIB) eigenvalue analysis of this system indicates that 28 generators have eigenvalues with real components less than -500. The smallest is around -2600. The eigenvalues are mostly associated with the EXST1 exciter model, a common exciter model used in the WECC case. It covers more than 30% of the total. The large negative eigenvalues represent extremely fast modes. For that reason, explicit methods require very small integration time steps to avoid numerical instability.

This chapter presents an algorithm for improving explicit transient stability solutions, increasing the solution speed without loss in accuracy. It investigates the conditions in which the fast modes of the EXST1 exciter model can be neglected or must be preserved. Based on experiment results, this chapter presents a practical way to determine when fast modes can be removed and a method to eliminate the modes from system equations. When fast modes can be ignored, a simpler model with those modes removed replaces the original model and larger time steps decrease the computational burden. Otherwise, the original model is used to maintain a high level of simulation accuracy.

Chapter 4 is organized as follows. Section 4.2 presents a brief description of the numerical integration methods employed in this dissertation. The problem definition is presented in Section 4.3. Section 4.4 proposes the new methodology to reduce the computational requirement. In Section 4.5, simulation results using the GSO 37-bus and the WECC system cases are presented. Finally, a summary is provided in Section 4.6.

4.2 Numerical Integration Method

4.2.1 Explicit numerical integration method

An example of an explicit numerical integration method is the second-order Runge-Kutta method (RK2). The RK2 is the main numerical integration scheme used in some commercial transient simulation packages [63]. This method is based on Heun's method which has a similar motivation to Taylor series expansion [69]. Given an ODE $\dot{x} = f(x,t)$, it approximates a real solution with the following form.

$$x_{n+1} = x_n + h * (\frac{1}{2}k_1 + \frac{1}{2}k_2) \tag{4.1}$$

where

$$k_1 = f(x_n, t_n)$$
$$k_2 = f(x_n + hk_1, t_n + h)$$
$$h : \text{integration time step}$$

With the simplest test equation $\dot{x} = \lambda x$, the region of stability is given by (4.2) and Fig. 4.1 shows the region.

$$|1 + h\lambda + \frac{1}{2}(h\lambda)^2| < 1 \tag{4.2}$$

For a real valued λ, the region of stability is $-2 < h\lambda < 0$. For example, when the minimum eigenvalue of a system is -2400, the time step required for numerical stability must be smaller than 0.00083 seconds (0.05 cycles).

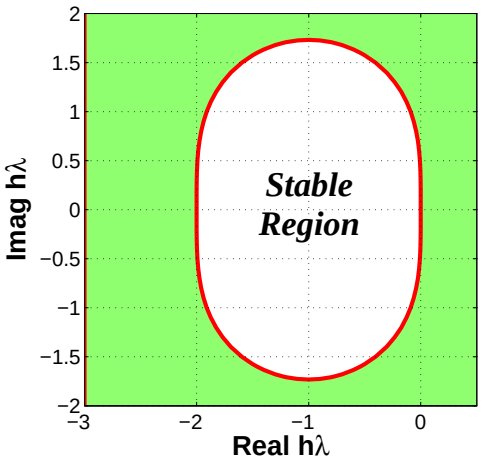

Figure 4.1: Region of stability of the RK2 method

4.2.2 Multirate method

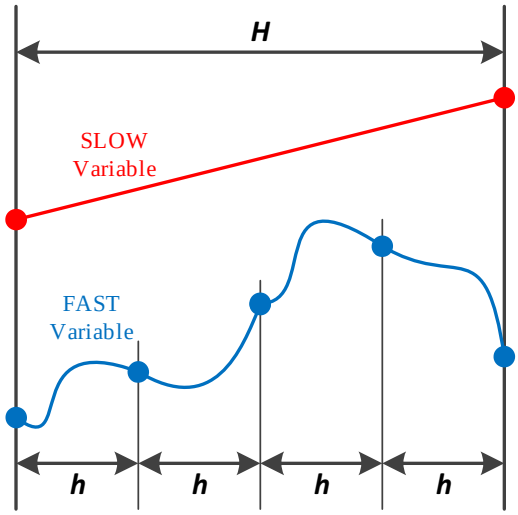

Figure 4.2: Multirate method implementation

The multirate method uses multiple different time steps in the numerical integration scheme. Figure 4.2 shows the process. For the fast-changing variables, a small time step (h) is used, while for the relatively slower changing variables, a multiple of the small time step (H) is used. For the example shown in Fig. 4.2, the ratio of the fast time step to the slow time step is 4.

The equations for the fast-changing variables must be solved at points where the slower ones are not solved. In these equations, linear interpolated values are used for the slow variables [68].

4.3 Problem Definition

4.3.1 WECC system and EXST1 exciter model

The exciter model is a primary source of fast dynamics and mainly used to control a machine terminal voltage and the reactive power dynamics [2]. A number of different exciter models are used, but a small number of them account for the extremely fast modes. In the WECC study case considered here, 28 generators show eigenvalues with real components less than -500 and all of the smallest eigenvalues are associated with the EXST1 model. The WECC case has a total of 2446 exciters, with the EXST1 model, the most common, used with about one-third of the models. The participation factors identify that those modes are mostly contributed by exciter state, V_A and the state V_A does not participate in other modes. Therefore, eliminating the eigenvalues related to the dynamic state from the system equations does not change other eigenvalues.

4.3.2 EXST1 model reduction

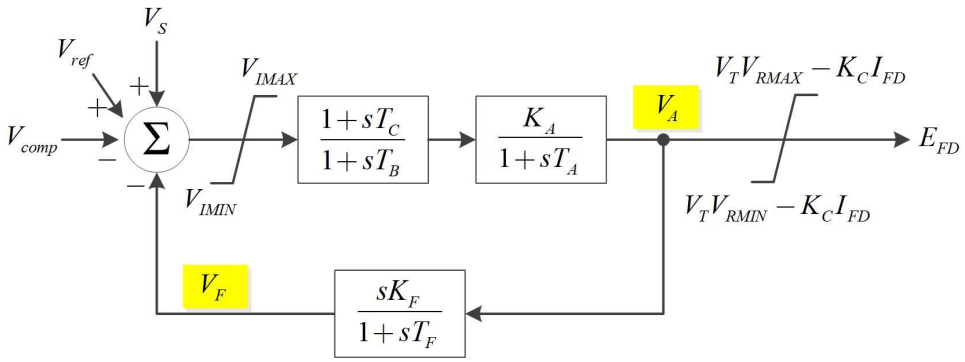

Figure 4.3: EXST1 exciter model block diagram

Figure 4.3 shows the block diagram of the EXST1 exciter model [70]. Due to the differential feedback block, the closed-loop transfer function shows a very small eigenvalue. The overall closed-loop transfer function is described by (4.3).

$$
\begin{aligned}
T(s) &= \frac{V_A}{(V_S + V_{ref} - V_{comp})} \\
&= \frac{K_A(1+sT_C)(1+sT_F)}{\left(\begin{array}{l} T_AT_BT_Fs^3 \\ +(T_AT_B + T_AT_F + T_BT_F + K_AT_FT_C)s^2 \\ +(T_A + T_B + T_F + K_AK_F)s + 1 \end{array} \right)} \\
&= \frac{K_A(1+sT_C)(1+sT_F)}{T_AT_BT_F(s-p_1)(s-p_2)(s-p_3)}
\end{aligned}
\tag{4.3}
$$

where p is the root of the denominator and $p_1 < p_2 < p_3 < 0$.

When the pole (p_1) associated with the very fast dynamics is eliminated from the closed-loop transfer function, the reduced transfer function is given in the following form.

$$
\begin{aligned}
T_{reduction}(s) &= \frac{V_A}{(V_S + V_{ref} - V_{comp})} \\
&= \frac{K_A(1+sT_C)(1+sT_F)}{T_A T_B T_F(-p_1)(s-p_2)(s-p_3)} \\
&= \frac{K_A(1+sT_C)(1+sT_F)}{(1-s/p_2)(1-s/p_3)}
\end{aligned}
\tag{4.4}
$$

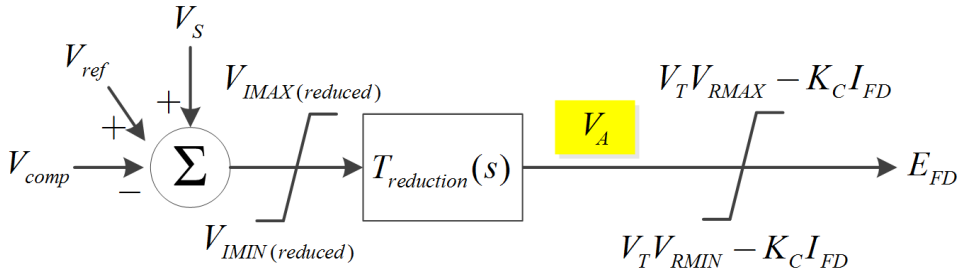

Figure 4.4: Block diagram of the reduced EXST1 exciter

The reduced EXST1 exciter model is shown in Fig. 4.4. In order to maintain the same limit function, the V_{IMAX} and V_{IMIN} values need to be modified. As shown in (4.5), the state V_F can be calculated at every simulation time step using the feedback transfer function with state V_A. New limits of the reduced model are simply updated by adding the V_F to those of the original model and it is shown in (4.6) and (4.7). The update is done once per time step, not at the subinterval time step.

$$
V_F = \frac{sK_F}{1+sT_F} V_A \tag{4.5}
$$

$$
V_{IMAX(reduced)} = V_{IMAX} + V_F \tag{4.6}
$$

$$
V_{IMIN(reduced)} = V_{IMIN} + V_F \tag{4.7}
$$

4.3.3 Comparison between the original and the reduced

Simulation results are compared using the original EXST1 model and the reduced one. The EXST1 model parameters for the simulations are presented in Appendix A.2.

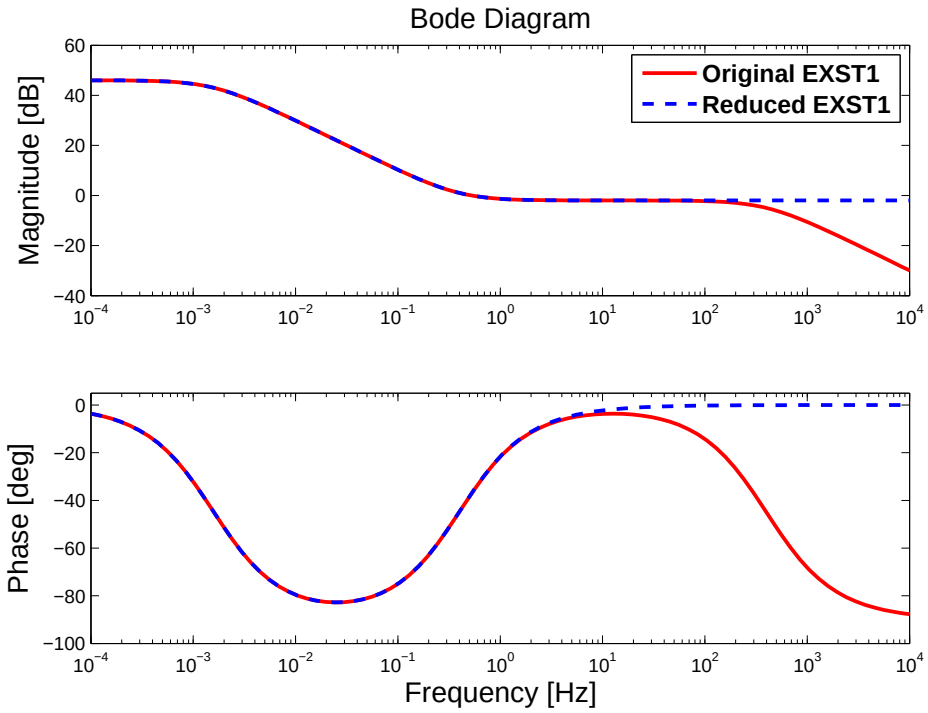

Figure 4.5: Bode plot of EXST1 exciter and its reduction

Figure 4.5 shows the Bode plots of the transfer functions of both the original and the reduced EXST1 models. The reduced model function is identical to the original model in the low-frequency range. Therefore, the reduced EXST1 model can take the place of the original model if the exciter input does not experience abrupt change.

On the other hand, in the high-frequency range, the difference is significant. Certain factors of the exciter inputs, such as the magnitude of voltage deviation and duration, bring about differences in the response of the original and the reduced models. The dependency on these factors is studied by ap-

plying a rectangular pulse which has a wide frequency spectrum to the V_{comp} of the original and the reduced models. The amplitude (A) and duration (D) in seconds of the pulse are varied for comparison. The difference is measured by the mean squared errors (MSE) shown in (4.8).

$$MSE = \frac{1}{N}\sum_{i=1}^{N}(x_{original} - x_{reduced})^2 \tag{4.8}$$

where N is the number of simulation time steps and x is time-series data compared.

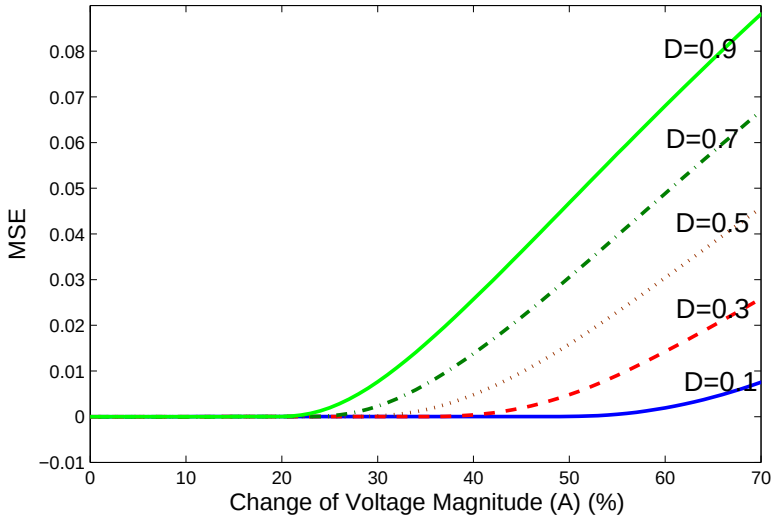

Figure 4.6: Simulation comparison with voltage magnitude deviation and duration

Figure 4.6 shows the MSE over a range of voltage magnitude deviation for a number of D values. It can be seen that the MSE is negligible when the amount of voltage deviation is less than 20% regardless of the duration. Therefore, the original EXST1 model can be switched to the reduced model if the input voltage deviation is small.

4.4 Proposed Method

In the proposed approach, a dynamic simulation begins with the reduced exciter model and dynamically switches back to the original model during simulation if the exciter input does not satisfy the model reduction conditions. Figure 4.7 depicts the procedure in the form of a flowchart.

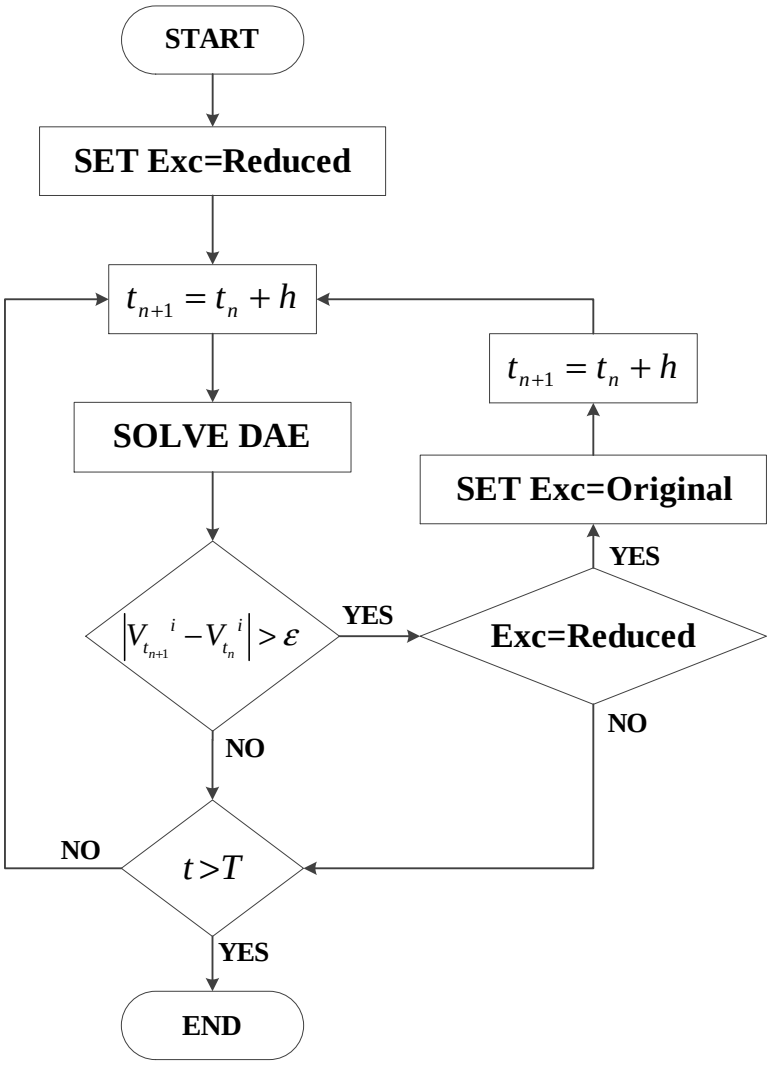

Figure 4.7: Proposed model complexity reduction method

The conditions are monitored at every integration time step by calculating the voltage deviation at generator terminals where the EXST1 exciter is placed. When it is over a certain threshold (ϵ) at a time instant (t_{n+1}), the proposed method switches from the reduced model to the original model in order to maintain the necessary simulation accuracy. From trial simulations based on Fig. 4.6, when the threshold is set to 10%, a satisfactory agreement between the original model and the reduced model is achieved. When the switching happens, the calculated values with the reduced model at the time instant (t_{n+1}) are neglected and the proposed approach performs the numerical integration again with the original model at the time instant. The integration at t_{n+1} requires all dynamic states of the original model at the previous time step (t_n). However, some of these states have not been computed because the reduced model has been used. The state V_A with the reduced model is set equal to that of the original model before the violation. As mentioned in Section 4.3, the proposed method updates the state V_F to keep the same limits. The other states at t_n can be obtained using the original exciter dynamic equations with the states V_F and V_A updated continuously.

4.5 Case Study

The proposed approach is implemented in the transient stability package, PowerWorld simulator [63]. Case studies are performed with the GSO 37-bus case and the WECC system in order to validate performance of the proposed method. Before the case studies, FFT analysis shows that fault type and location are related to the range of frequency spectrum and the degree of voltage deviation.

4.5.1 FFT analysis with faults

During generator or load outage, the key dynamics are driven by the device inertia and the response of generator governors. A detailed exciter model may not be necessary and it may be replaced by a much simpler model. Faults related to bus voltage magnitude or reactive power dynamics may be closely related to the exciter function. An initial investigation is performed to find the types of faults that result in high-frequency components in generator terminal voltage. The investigation is done using the simple power system case shown in Fig. 4.8.

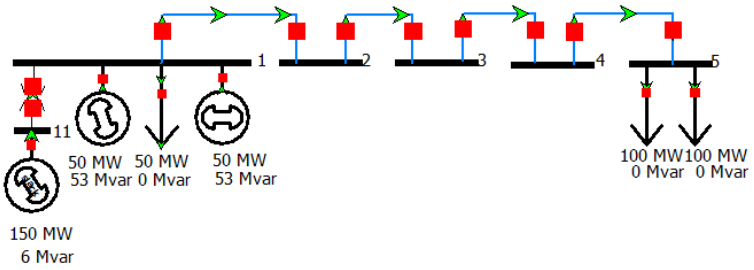

Figure 4.8: Simple test case for FFT analysis

A generator, a load outage, a three-phase bus to ground fault at bus 1 and a line 1-2 to ground fault are compared. The FFT analysis is conducted on bus 1 voltage magnitude data. As shown in Fig. 4.9, the bus or line to ground fault results in a bus voltage with the greatest magnitude over a wide frequency range. This is because the bus voltage experiences abrupt rectangular change when the faults occur. Conversely, for a generator or load outage, the magnitude for frequency over 10 Hz is negligible. Therefore, for the following case studies, a generator outage is used to demonstrate a situation where high-frequency components are not injected.

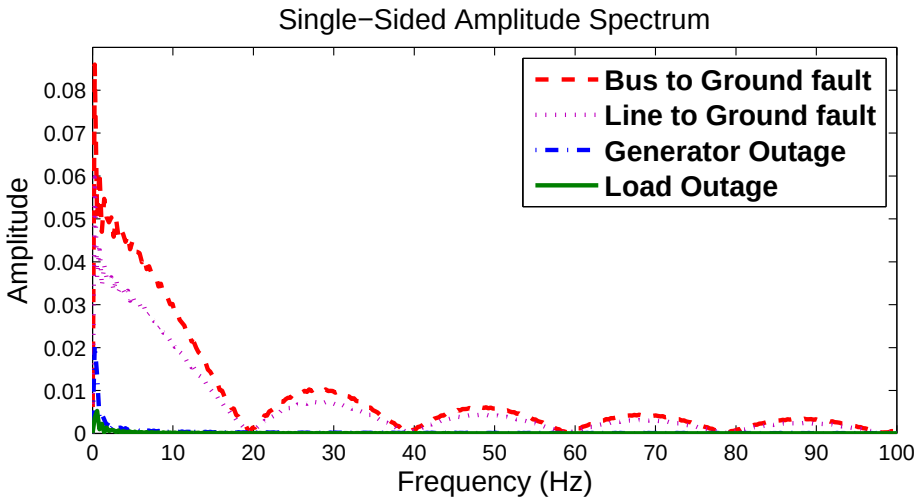

Figure 4.9: FFT analysis with different types of fault

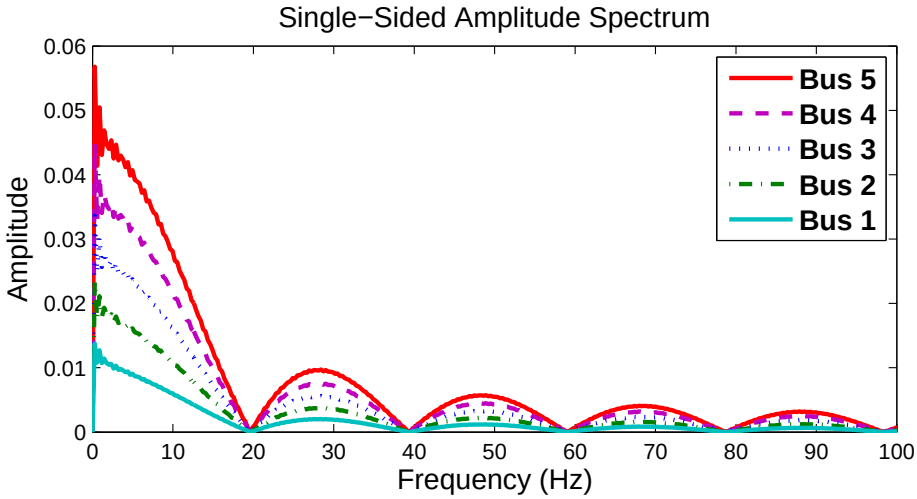

Figure 4.10: FFT analysis with a bus to ground fault

When a bus to ground fault occurs, the magnitude of voltage deviation is dependent upon the electrical distance between the bus fault location and the neighboring buses. When a bus fault occurs far from a bus, its impact on changing the bus voltage magnitude is lessened. A bus to ground fault is simulated at bus 5 of the system in Fig. 4.8. The FFT results of the bus voltage magnitude at the five different buses are shown in Fig. 4.10. It is seen that the farther a fault location is from a bus, the less the effect on the

bus voltage. For the following case studies, the amount of voltage deviation is considered by changing the bus to ground fault location.

4.5.2 GSO 37-bus case

The GSO 37-bus case is shown in Fig. 4.11. The case contains 57 branches, 9 generators and 25 loads [71]. For test purposes, the parameters of the two EXST1 exciters at bus 28 are changed as shown in Appendix A.2. SMIB eigenvalue analysis indicates that two large negative eigenvalues, both at -2102, originate from the exciter models.

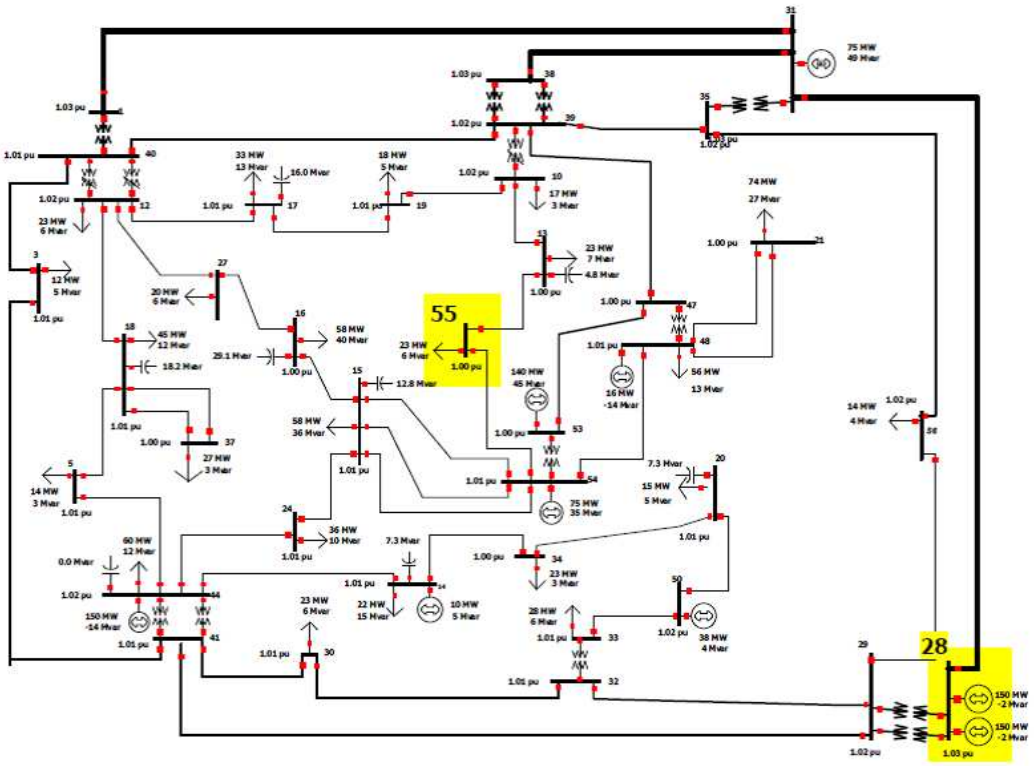

Figure 4.11: GSO 37-bus case

The performance is evaluated by comparing simulation results using the proposed method with using the conventional method. Three different faults are tested to consider the situations related to the proposed criteria. In the first test, a generator outage at bus 28 is applied so as to consider the condition in which the generator terminal voltage contains mostly low-frequency components. Two remaining tests simulate bus to ground faults at buses 28 and 55 to consider different magnitudes of voltage deviation.

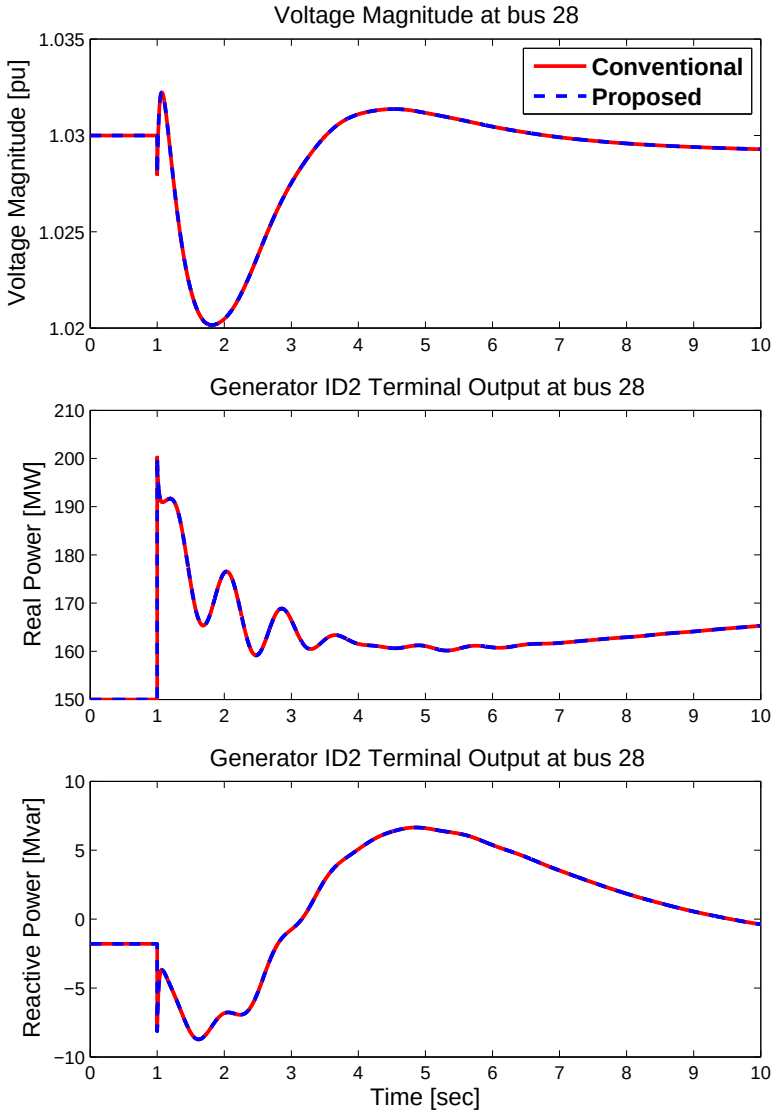

Figure 4.12: Simulation for Generator ID1 outage at bus 28

Table 4.1: Mean squared error for generator ID1 outage at bus 28

	MSE
Bus 28 Voltage Magnitude (pu)	6.36e-13
Gen ID2 Real Power (MW)	4.73e-8
Gen ID2 Reactive Power (Mvar)	4.01e-6

The results of the generator outage test are presented in Fig. 4.12. The results show bus voltage magnitude, both the real and reactive power output of generator ID2 at the bus 28 when generator ID1 is tripped at 1 second. The MSE of the responses over the period from 0 to 10 seconds is shown in Table 4.1. The simulation results with the reduced EXST1 are virtually identical to those with the original model. This validates the claim that the large negative eigenvalues from the EXST1 exciter model can be neglected when a high-frequency input is not applied.

The next comparison is made with the simulation of a solid bus to ground fault. A three-phase bus to ground fault is applied at bus 55 at 1 second and it is cleared at 1.1 seconds. Figure 4.13 shows the simulation comparisons and Table 4.2 shows the MSE calculation over the period from 0 to 10 seconds. The differences are small enough to be neglected. It can be understood that the fault location, bus 55 is far enough from the location of the EXST1 exciter, bus 28. The magnitude of voltage deviation at bus 28 is not large enough to produce a significant difference between the results using the original EXST1 exciter model and the reduced model. Thus, even if the high-frequency components are injected to the exciter model, if the magnitude of those components is small, the very fast mode of the EXST1 model can be eliminated, while maintaining accurate system responses.

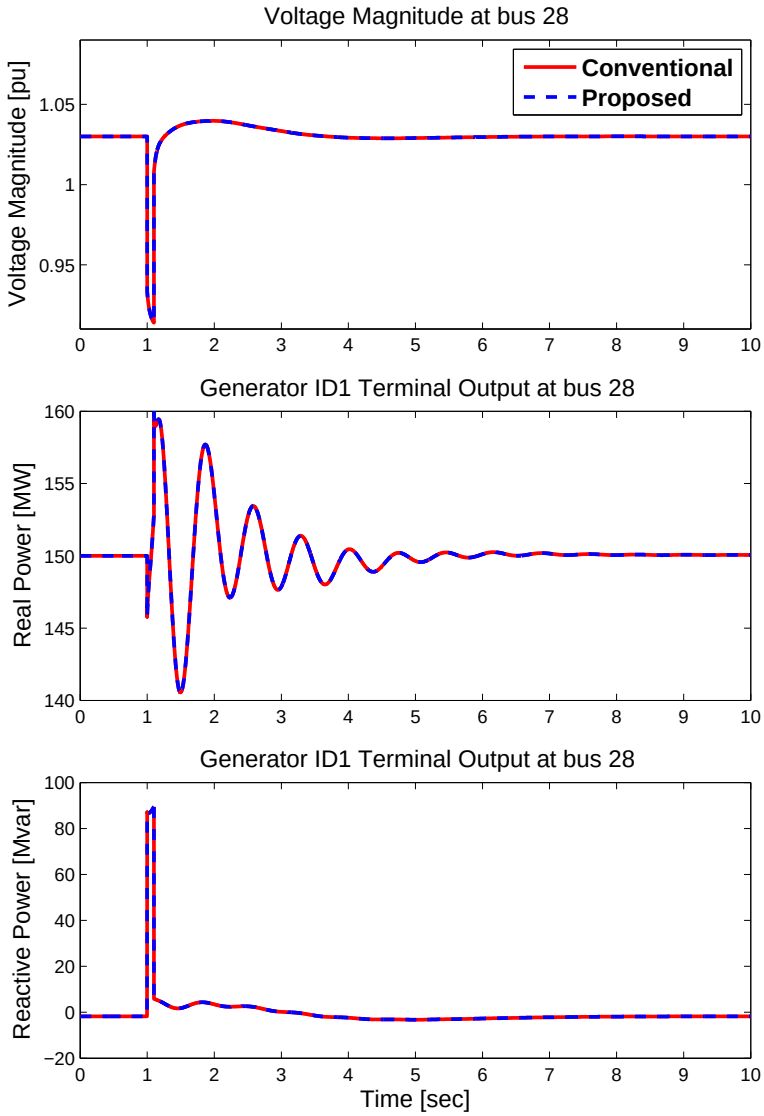

Figure 4.13: Simulation for bus to ground fault at bus 55

Table 4.2: Mean squared error for bus to ground fault at bus 55

	MSE
Bus 28 Voltage Magnitude (pu)	1.42e-11
Gen ID1 Real Power (MW)	3.82e-6
Gen ID1 Reactive Power (Mvar)	1.50e-5

Finally, the dynamic responses of a three-phase bus to ground fault at bus 28 simulated at 1 second and cleared at 1.05 seconds are presented in Fig.

4.14. The bus voltage experiences abrupt variation, well over the threshold (10%). The proposed method restores the original exciter model and shows the same responses as the conventional method. For comparison, the simulation results with the reduced exciter model are shown in Fig. 4.14 and the differences are evident. The MSE between using the original exciter model and using the reduced model is presented in Table 4.3. And the results in Fig. 4.14 show a faster response using the reduced model over the original

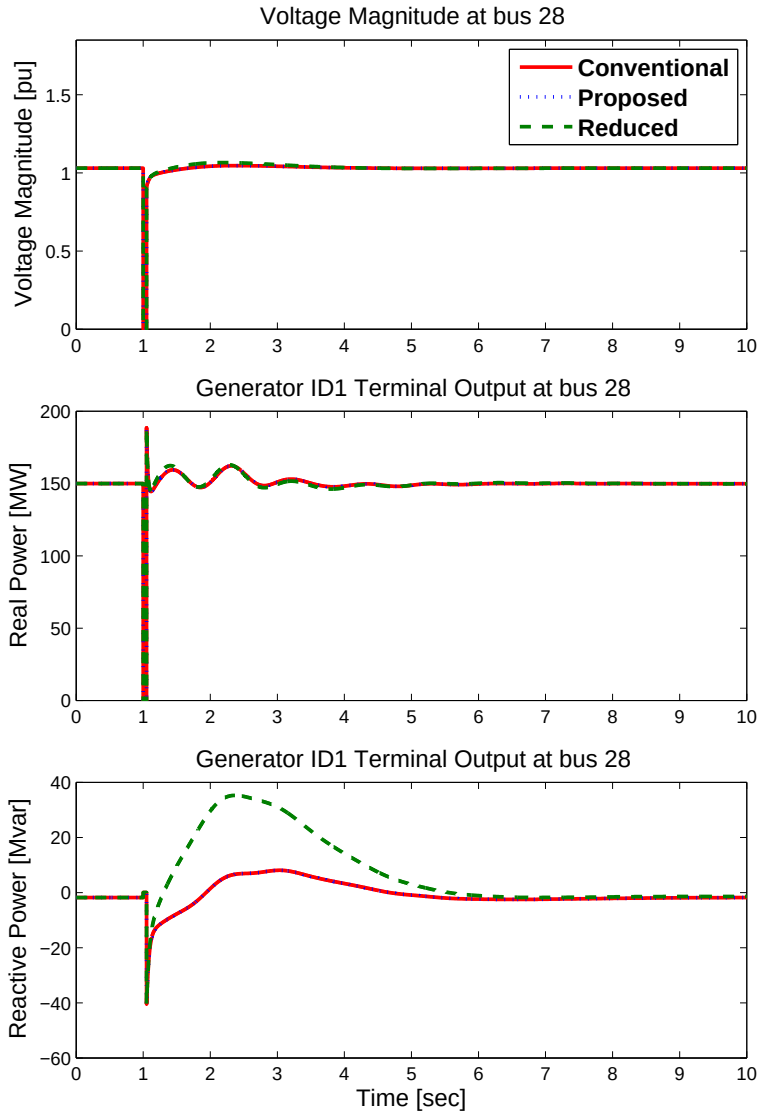

Figure 4.14: Simulation for bus to ground fault at bus 28

model. This is because the magnitude of the transfer function of the reduced model in the high-frequency range is larger than that of the original model.

Table 4.3: Mean squared error for bus to ground fault at bus 28

	MSE
Bus 28 Voltage Magnitude (pu)	6.57e-5
Gen ID1 Real Power (MW)	1.0245
Gen ID1 Reactive Power (Mvar)	158.81

Table 4.4 shows the computation time and integration time step of three different simulation approaches. Each integration time step is the maximum allowable step size to avoid numerical instability. A simulation of the bus to ground fault at bus 55 is performed. The computation time is an average execution time of multiple 10-second simulations. The proposed method with the reduced exciter model decreases the simulation time by approximately 98% compared to that of the single-rate method with the original exciter model. Compared to the multirate method, the presented approach shows a 7% computation time saving. This saving is due to the fact that integration associated with the fast dynamics are not performed. As demonstrated in Table 4.2 and Fig. 4.13, the proposed approach preserves a high accuracy level.

Table 4.4: Computation time for the GSO 37-bus case

Method Used	Exciter Model	Numerical Integration	Int. Time Step (cycle)	Time to Solve (sec)
Conventional	Original	Single-rate	0.05	47.99
		Multi-rate	2.4	1.08
Proposed	Reduced	Single-rate	2.4	1.01

4.5.3 WECC case

The WECC system consists of 17,710 buses, 3470 generators and 8493 individual loads. To validate the proposed method, all negative eigenvalues with real component magnitude greater than 500 and associated with the EXST1 model are eliminated. In this case, a total of 28 original EXST1 exciter models are replaced with the reduced model. Simulation results using the conventional method and using the proposed approach are compared. Similar faults to those in the GSO 37-bus case are applied.

First, a generator outage is simulated at generator ID4 at bus A, which contributes to one of the smallest eigenvalues in the system. Figure 4.15 shows bus voltage magnitude, the real and reactive power output of generator ID1 at the bus A. As expected, the responses from the reduced model match those from the original model. The MSE are evaluated for the 5-seconds simulation and are presented in Table 4.5.

Table 4.5: Mean squared error for generator ID4 outage at bus A

	MSE
Bus A Voltage Magnitude (pu)	2.09e-12
Gen ID1 Real Power (MW)	3.7e-7
Gen ID1 Reactive Power (Mvar)	5.1e-9

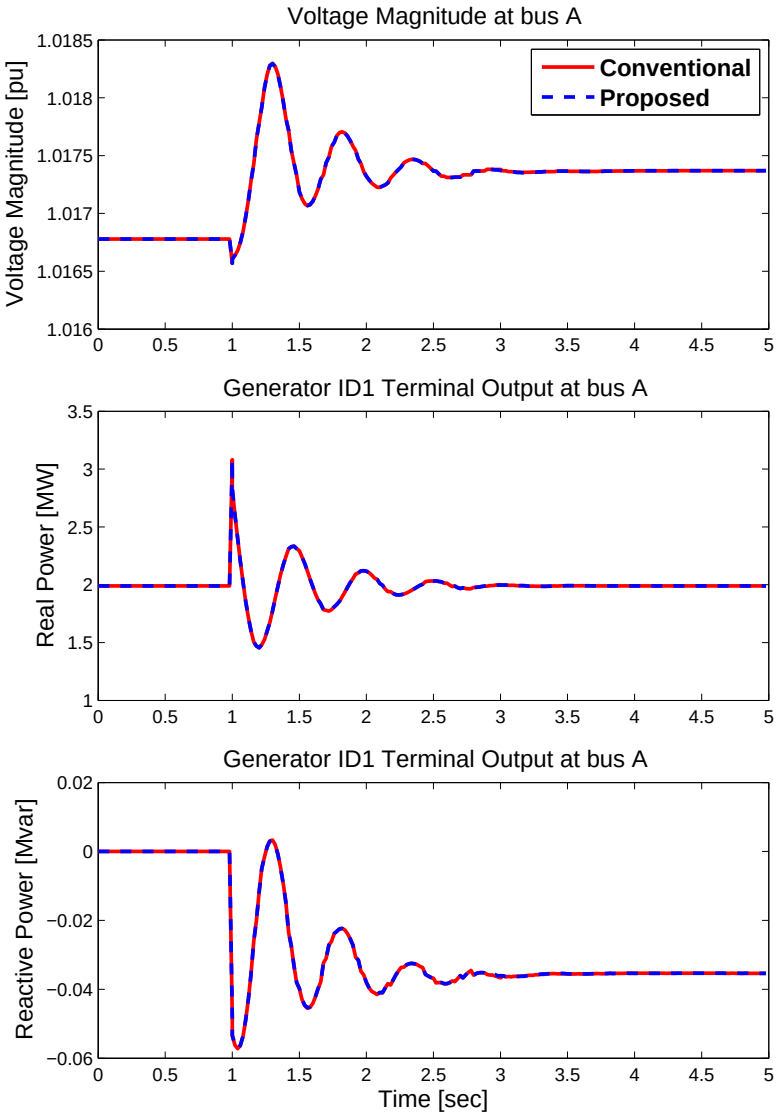

Figure 4.15: Simulation for Generator ID4 outage at bus A

Generator ID1 at bus B also participates significantly in one of the smallest negative eigenvalues. To consider the amount of voltage deviation, a solid bus to ground fault is simulated at bus C which neighbors the bus B at 1 second. At 1.1 seconds, the fault is cleared. The bus voltage magnitude, and both the real and reactive power output of generator ID1 at bus B using the two approaches are compared in Fig. 4.16. As shown in Table 4.6, the MSE difference is very slight and can be neglected.

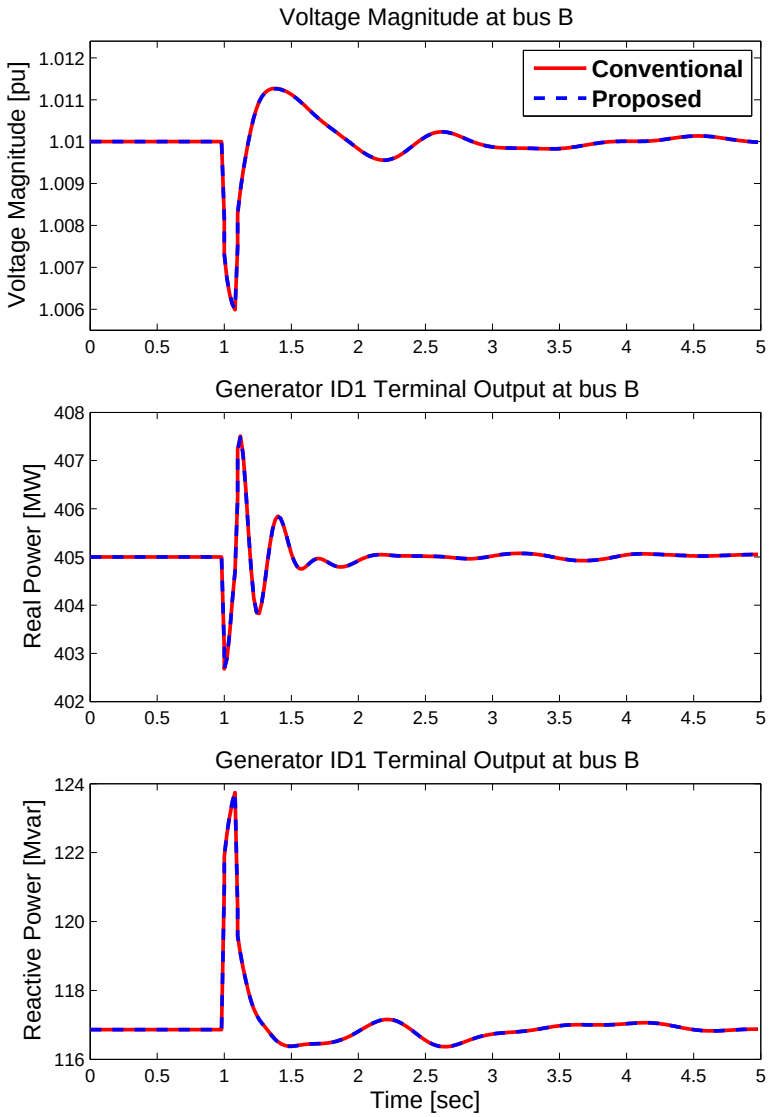

Figure 4.16: Simulation for bus to ground fault at bus C

Table 4.6: Mean squared error for bus to ground fault at bus C

	MSE
Bus A Voltage Magnitude (pu)	6.96e-12
Gen ID1 Real Power (MW)	1.67e-5
Gen ID1 Reactive Power (Mvar)	1.83e-5

The simulation results of a bus to ground fault applied to bus B at 1 second and cleared at 1.1 seconds are shown in Fig. 4.17. When this fault is simulated, the proposed method changes the reduced exciter model to the original model because the requirement is violated. For comparison, the simulation result with the reduced model is also shown in Fig. 4.17. The MSE between using the original model and using the reduced one is shown in Table 4.7 and it shows obvious distinction.

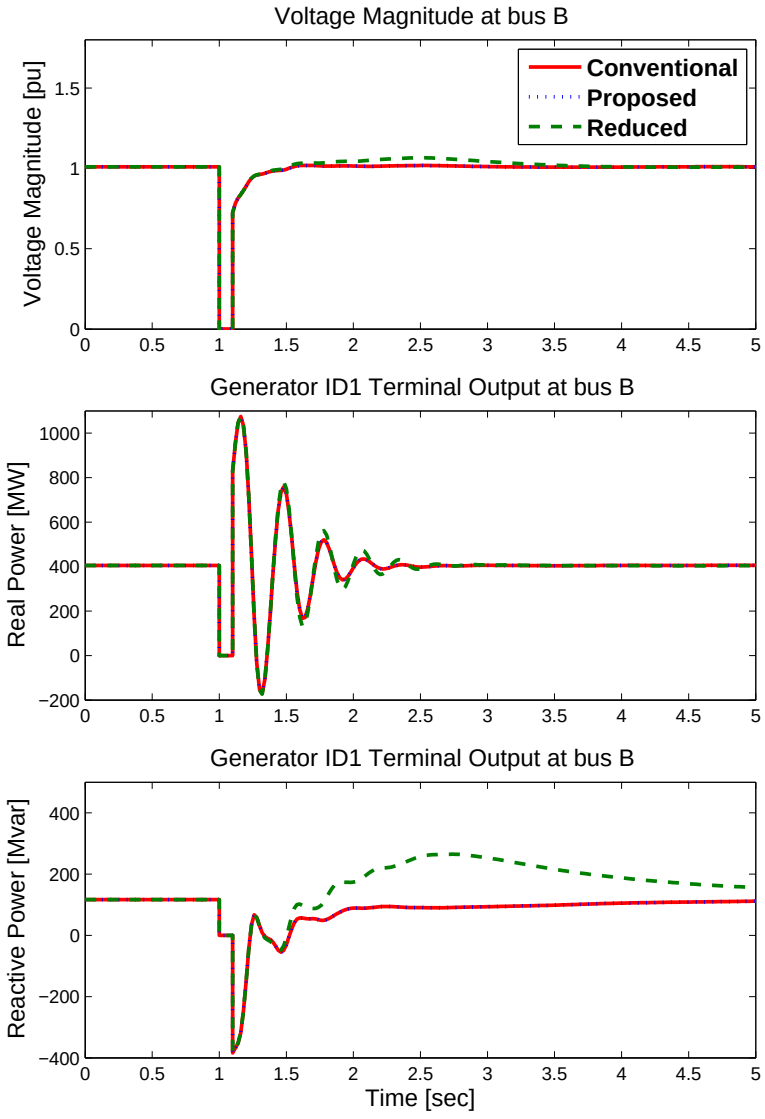

Figure 4.17: Simulation for bus to ground fault at bus B

Table 4.7: Mean squared error for bus to ground fault at bus B

	MSE
Bus A Voltage Magnitude (pu)	4.40e-4
Gen ID1 Real Power (MW)	124.92
Gen ID1 Reactive Power (Mvar)	8582.6

The computation times with three different simulation approaches depending on the exciter model and the integration method are compared in Table 4.8. Simulations is performed with the maximum step size of each approach to prevent the numerical instability. It is measured for when the bus to ground fault is at the bus C and the simulation ends at 5 seconds. The computation time is obtained by running the simulations multiple times. Compared to the single-rate method with the original exciter model, the simulation time of the proposed method with the reduced model decreases by approximately 83% and this results from a larger integration time step. About 7% of computation time is reduced by using the proposed method compared to the multirate approach with the original exciter model. These exciters are being simulated with quite small subintervals because of the fast dynamics from the EXST1 model. Some commercial packages reduce the time step for the models by a factor of 64 or 128. The reduced model does not require the small time steps because the fast modes are eliminated.

Table 4.8: Computation time for the WECC case

Method Used	Exciter Model	Numerical Integration	Int. Time Step (cycle)	Time to Solve (sec)
Conventional	Original	Single-rate	0.04	487.3
		Multi-rate	0.24	89.9
Proposed	Reduced	Single-rate	0.24	83.1

4.6 Summary

Power system transient stability analysis is computationally demanding. However, much of the computation that occurs during a transient simulation is wasted effort and does not have any impact on the solution outcome. Therefore, the main challenge for faster transient stability simulation is to determine how the system models can be reduced, while maintaining the correct system responses. It is explored that an excitation of fast modes related to the EXST1 exciter model is dependent on a large and sudden transition of the generator terminal voltage. The proposed approach dynamically switches between the EXST1 exciter model and the reduced model, for which large negative eigenvalues are eliminated. Larger integration time steps and the removal of subinterval integrations decrease the execution time of power system transient simulations without numerical instability. This method is an advanced dynamic simulation algorithm which provides a fast explicit transient solution without sacrificing simulation accuracy.

CHAPTER 5

CONCLUSIONS

5.1 Summary

This dissertation explores three approaches to enhance the computational efficiency for power flow and transient stability analyses. The proposed methods have been demonstrated on power system test cases to validate the performance in terms of computation time and simulation accuracy. These methods can be utilized in a variety of power system applications. It is expected that the proposed approaches would be a promising solution for advanced power system study.

In Chapter 2, the importance of power flow analysis and its fast solution has been addressed. A new power flow algorithm has been proposed by combining the detailed ac model with the less detailed dc model. The advanced power flow model achieves a fast solution, about ten to thirty times faster for LU factorization and six to fifteen times faster for forward and backward substitution compared to using the ac model alone, without sacrificing accuracy in areas of interest. It can be used for any size of power system. More benefits in terms of speed can be achieved with larger power system cases and higher dimensionality of the external system compared to the internal one. In contrast to the network equivalent technique, the approach still includes the external system, thus is able to capture variations there.

In Chapter 3, an alternative method that speeds up transient stability sim-

ulations while still maintaining a high level of simulation accuracy has been proposed. It is based on the fact that the reactive power tends to be more localized compared to real powers. In the area of interest, where the disturbances are applied and accurate simulation outcomes are required, both real and reactive power equations should be considered to represent power system dynamics correctly, while real power equations would be enough in the more remote areas where real power dynamics are dominant. The proposed approach thus formulates power flow equations for transient stability simulation by combining the full ac and dc models. A detailed ac model, including nonlinear real and reactive power equations, is used in the internal system, while a simpler dc model is used in the external system. The real power losses ignored by the standard dc model are made up for in the external system by using the initial power flow solutions. The test simulations performed with the IEEE 118-bus system have confirmed that the proposed method achieves faster and accurate solution.

Finally, Chapter 4 presents a model reduction approach focusing on the EXST1 exciter model. It is explored that an excitation of fast modes related to the EXST1 exciter model is dependent on a large and sudden transition of the generator terminal voltage. The proposed approach dynamically switches between the EXST1 exciter model and the reduced model, for which large negative eigenvalues are eliminated. Larger integration time steps and the removal of subinterval integrations decrease the execution time of power system transient simulations without numerical instability. This method is an advanced dynamic simulation algorithm which provides a fast explicit transient solution without sacrificing simulation accuracy.

5.2 Future Research

For future research to further advance the proposed methods, the following work is suggested.

5.2.1 Mixed power flow analysis

The standard dc power flow model applied to the external system is inherently approximate and its solution accuracy is very problem dependent. The neglect of real power losses would bring about total real power imbalance. These shortcomings with the dc model can be overcome by developing a linearized power flow model, which can be obtained from a initial power flow solution. The accuracy in the internal system can thus be improved without additional computational expenses.

5.2.2 Mixed transient stability analysis

First, the dc model used in the external system neglects voltage magnitude deviation and reactive power balance equations. Fast dynamics in power system equations are mostly originated from controllers associated with those reactive power and voltage magnitude terms. Even larger computational benefits could thus be achieved with the mixed transient stability method if we are able to allow for larger time step solutions in the external system.

Second, further research can be carried on by incorporating higher-order machine models instead of the classical machine model used in this dissertation and by exploring how to reduce the complicated machine model to a simple one in the external system.

5.2.3 Exciter model complexity reduction

The proposed method deals with the EXST1 exciter model which is the most common in the WECC system. Other types of exciter models, which are associated with another large negative eigenvalues, can be reduced with the same approach used in this dissertation. Such models would have a similar block diagram to the EXST1 exciter because the differential feedback loop produces the large negative eigenvalues.

APPENDIX A

TEST SYSTEM DATA

A.1 Dynamic Parameters of Chapter 3

Table A.1: Machine parameters for the IEEE 118-bus system (Machine base: 100 MVA)

Generator Number	H	X_{dp}	D	Generator Number	H	X_{dp}	D
10	5.66	0.059	1	65	7.41	0.067	1
12	9.97	0.22	1	66	7.41	0.067	1
25	8.24	0.139	1	69	5.26	0.053	1
26	6.01	0.096	1	80	5.26	0.053	1
31	12.37	0.247	1	87	12.37	0.247	1
46	12.37	0.247	1	89	4.64	0.047	1
49	8.24	0.139	1	100	8.26	0.095	1
54	9.97	0.22	1	103	9.97	0.22	1
59	7.93	0.153	1	111	9.97	0.22	1
61	7.93	0.153	1				

Table A.2: TGOV1 model parameters (all generators have the same parameters)

R	T1	T2	T3	Vmax/Vmin
0.05	0.5	3	10	7/0

A.2 Dynamic Parameters of Chapter 4

Table A.3: EXST1 exciter model parameters

$V_{imax} = 10$	$V_{imin} = -10$	$T_C = 1$	$T_B = 1$
$K_A = 200$	$T_A = 0.01$	$K_F = 0.04$	$T_F = 0.4$
$V_{rmax} = 3.6$	$V_{rmin} = 0$	$K_C = 0$	

REFERENCES

[1] L. Wang and K. Morison, "Implementation of online security assessment," *Power and Energy Magazine, IEEE*, vol. 4, no. 5, pp. 46–59, Sept 2006.

[2] P. Kundur, N. J. Balu, and M. G. Lauby, *Power System Stability and Control*. New York: McGraw-Hill, 1994.

[3] D. Tylavsky and A. Bose, "Parallel processing in power systems computation," *Power Systems, IEEE Transactions on*, vol. 7, no. 2, pp. 629–638, May 1992.

[4] R. Green, L. Wang, and M. Alam, "High performance computing for electric power systems: Applications and trends," in *Power and Energy Society General Meeting, 2011 IEEE*, July 2011, pp. 1–8.

[5] J. Q. Wu, A. Bose, J. A. Huang, A. Valette, and F. Lafrance, "Parallel implementation of power system transient stability analysis," *Power Systems, IEEE Transactions on*, vol. 10, no. 3, pp. 1226–1233, Aug 1995.

[6] J. Shu, W. Xue, and W. Zheng, "A parallel transient stability simulation for power systems," *Power Systems, IEEE Transactions on*, vol. 20, no. 4, pp. 1709–1717, Nov 2005.

[7] S. Huang, Y. Chen, C. Shen, W. Xue, and J. Wang, "Feasibility study on online DSA through distributed time domain simulations in WAN," *Power Systems, IEEE Transactions on*, vol. 27, no. 3, pp. 1214–1224, Aug 2012.

[8] J. B. Ward, "Equivalent circuits for power-flow studies," *Electrical Engineering*, vol. 68, no. 9, pp. 794–794, Sept 1949.

[9] S. Deckmann, A. Pizzolante, A. Monticelli, B. Stott, and O. Alsac, "Studies on power system load flow equivalencing," *Power Apparatus and Systems, IEEE Transactions on*, vol. PAS-99, no. 6, pp. 2301–2310, Nov 1980.

[10] F. F. Wu and A. Monticelli, "Critical review of external network modelling for online security analysis," *International Journal of Electrical Power & Energy Systems*, vol. 5, no. 4, pp. 222–235, 1983.

[11] S. Deckmann, A. Pizzolante, A. Monticelli, B. Stott, and O. Alsac, "Numerical testing of power system load flow equivalents," *Power Apparatus and Systems, IEEE Transactions on*, vol. PAS-99, no. 6, pp. 2292–2300, Nov 1980.

[12] A. Monticelli, S. Deckmann, A. Garcia, and B. Stott, "Real-time external equivalents for static security analysis," *Power Apparatus and Systems, IEEE Transactions on*, vol. PAS-98, no. 2, pp. 498–508, March 1979.

[13] P. Dimo, *Nodal Analysis of Power Systems*. Editura Academiei Republicii Socialisté România, 1975.

[14] T. Dy Liacco, S. Savulescu, and K. Ramarao, "An on-line topological equivalent of a power system," *Power Apparatus and Systems, IEEE Transactions on*, vol. PAS-97, no. 5, pp. 1550–1563, Sept 1978.

[15] X. Cheng and T. Overbye, "PTDF-based power system equivalents," *Power Systems, IEEE Transactions on*, vol. 20, no. 4, pp. 1868–1876, Nov 2005.

[16] H. Oh, "A new network reduction methodology for power system planning studies," *Power Systems, IEEE Transactions on*, vol. 25, no. 2, pp. 677–684, May 2010.

[17] J. Machowski, J. Bialek, and J. Bumby, *Power System Dynamics: Stability and Control*. Chichester, U.K.: Wiley, 2008.

[18] U. Annakkage, N. K. C. Nair, Y. Liang, A. Gole, V. Dinavahi, B. Gustavsen, T. Noda, H. Ghasemi, A. Monti, M. Matar, R. Iravani, and J. Martinez, "Dynamic system equivalents: A survey of available techniques," *Power Delivery, IEEE Transactions on*, vol. 27, no. 1, pp. 411–420, Jan 2012.

[19] J. Undrill and A. E. Turner, "Construction of power system electromechanical equivalents by modal analysis," *Power Apparatus and Systems, IEEE Transactions on*, vol. PAS-90, no. 5, pp. 2049–2059, Sept 1971.

[20] W. W. Price and B. A. Roth, "Large-scale implementation of modal dynamic equivalents," *Power Apparatus and Systems, IEEE Transactions on*, vol. PAS-100, no. 8, pp. 3811–3817, Aug 1981.

[21] E. Davison, "A method for simplifying linear dynamic systems," *Automatic Control, IEEE Transactions on*, vol. 11, no. 1, pp. 93–101, Jan 1966.

[22] I. Perez-Arriaga, G. Verghese, and F. Schweppe, "Selective modal analysis with applications to electric power systems, Part i: Heuristic introduction," *Power Apparatus and Systems, IEEE Transactions on*, vol. PAS-101, no. 9, pp. 3117–3125, Sept 1982.

[23] G. Verghese, I. Perez-Arriaga, and F. Schweppe, "Selective modal analysis with applications to electric power systems, Part ii: The dynamic stability problem," *Power Apparatus and Systems, IEEE Transactions on*, vol. PAS-101, no. 9, pp. 3126–3134, Sept 1982.

[24] G. Rogers, *Power System Oscilations*, ser. The Kluwer International Series in Engineering and Computer Science: Power Electronics and Power Systems. Boston: Kluwer Academic, 2000.

[25] R. Podmore, "Identification of coherent generators for dynamic equivalents," *Power Apparatus and Systems, IEEE Transactions on*, vol. PAS-97, no. 4, pp. 1344–1354, July 1978.

[26] A. Germond and R. Podmore, "Dynamic aggregation of generating unit models," *Power Apparatus and Systems, IEEE Transactions on*, vol. PAS-97, no. 4, pp. 1060–1069, July 1978.

[27] J. Chow, *Time-Scale Modeling of Dynamic Networks with Applications to Power Systems*, ser. Lecture Notes in Control and Information Sciences. Berlin: Springer-Verlag, 1982.

[28] J. H. Chow, *Power System Coherency and Model Reduction*. New York: Springer, 2013.

[29] J. Zaborszky, K.-W. Whang, G. Huang, L.-J. Chiang, and S.-Y. Lin, "A clustered dynamic model for a class of linear autonomous systems using simple enumerative sorting," *Circuits and Systems, IEEE Transactions on*, vol. 29, no. 11, pp. 747–758, Nov 1982.

[30] R. Nath, S. Lamba, and K. S. P. Rao, "Coherency based system decomposition into study and external areas using weak coupling," *Power Apparatus and Systems, IEEE Transactions on*, vol. PAS-104, no. 6, pp. 1443–1449, June 1985.

[31] F. Ma and V. Vittal, "Right-sized power system dynamic equivalents for power system operation," *Power Systems, IEEE Transactions on*, vol. 26, no. 4, pp. 1998–2005, 2011.

[32] J. Chow, R. Galarza, P. Accari, and W. Price, "Inertial and slow coherency aggregation algorithms for power system dynamic model reduction," *Power Systems, IEEE Transactions on*, vol. 10, no. 2, pp. 680–685, May 1995.

[33] W. Price, D. Ewart, E. M. Gulachenski, and R. Silva, "Dynamic equivalents from on-line measurements," *Power Apparatus and Systems, IEEE Transactions on*, vol. 94, no. 4, pp. 1349–1357, July 1975.

[34] J. Ramirez, "Obtaining dynamic equivalents through the minimization of a line flows function," *International Journal of Electrical Power & Energy Systems*, vol. 21, no. 5, pp. 365–373, 1999.

[35] P. Ju, L. Q. Ni, and F. Wu, "Dynamic equivalents of power systems with online measurements. Part 1: Theory," *Generation, Transmission and Distribution, IEE Proceedings*, vol. 151, no. 2, pp. 175–178, March 2004.

[36] D. Trudnowski, "Estimating electromechanical mode shape from synchrophasor measurements," *Power Systems, IEEE Transactions on*, vol. 23, no. 3, pp. 1188–1195, Aug 2008.

[37] A. Chakrabortty, J. Chow, and A. Salazar, "A measurement-based framework for dynamic equivalencing of large power systems using wide-area phasor measurements," *Smart Grid, IEEE Transactions on*, vol. 2, no. 1, pp. 68–81, March 2011.

[38] B. Stott, "Review of load-flow calculation methods," *Proceedings of the IEEE*, vol. 62, no. 7, pp. 916–929, July 1974.

[39] W. F. Tinney and C. Hart, "Power flow solution by Newton's method," *Power Apparatus and Systems, IEEE Transactions on*, vol. PAS-86, no. 11, pp. 1449–1460, Nov 1967.

[40] S. Iwamoto and Y. Tamura, "A load flow calculation method for ill-conditioned power systems," *Power Apparatus and Systems, IEEE Transactions on*, vol. PAS-100, no. 4, pp. 1736–1743, April 1981.

[41] J. Jardim and B. Stott, "Synthetic dynamics power flow," in *Power Engineering Society General Meeting, 2005. IEEE*, June 2005, pp. 479–484 Vol. 1.

[42] A. Wood and B. Wollenberg, *Power Generation, Operation, and Control*. New York: Wiley, 1996.

[43] B. Stott and O. Alsac, "Fast decoupled load flow," *Power Apparatus and Systems, IEEE Transactions on*, vol. PAS-93, no. 3, pp. 859–869, May 1974.

[44] B. Stott, J. Jardim, and O. Alsac, "Dc power flow revisited," *Power Systems, IEEE Transactions on*, vol. 24, no. 3, pp. 1290–1300, Aug 2009.

[45] P. H. Haley and M. Ayres, "Super decoupled loadflow with distributed slack bus," *Power Apparatus and Systems, IEEE Transactions on*, vol. PAS-104, no. 1, pp. 104–113, Jan 1985.

[46] D. Rajicic and A. Bose, "A modification to the fast decoupled power flow for networks with high r/x ratios," *Power Systems, IEEE Transactions on*, vol. 3, no. 2, pp. 743–746, May 1988.

[47] F. Yang, A. P. S. Meliopoulos, G. Cokkinides, and G. Stefopoulos, "Contingency simulation using single phase quadratized power flow," in *Probabilistic Methods Applied to Power Systems, 2006. PMAPS 2006. International Conference on*, June 2006, pp. 1–8.

[48] B. Borkowska, "Probabilistic load flow," *Power Apparatus and Systems, IEEE Transactions on*, vol. PAS-93, no. 3, pp. 752–759, May 1974.

[49] V. Miranda and J. Saraiva, "Fuzzy modelling of power system optimal load flow," in *Power Industry Computer Application Conference, 1991. Conference Proceedings*, May 1991, pp. 386–392.

[50] K. Kato, "External network modeling-recent practical experience," *Power Systems, IEEE Transactions on*, vol. 9, no. 1, pp. 216–228, Feb 1994.

[51] N. Balu, T. Bertram, A. Bose, V. Brandwajn, G. Cauley, D. Curtice, A. Fouad, L. Fink, M. Lauby, B. Wollenberg, and J. N. Wrubel, "On-line power system security analysis," *Proceedings of the IEEE*, vol. 80, no. 2, pp. 262–282, Feb 1992.

[52] T. Overbye, X. Cheng, and Y. Sun, "A comparison of the ac and dc power flow models for LMP calculations," in *System Sciences, 2004. Proceedings of the 37th Annual Hawaii International Conference on*, Jan 2004.

[53] K. Purchala, L. Meeus, D. Van Dommelen, and R. Belmans, "Usefulness of dc power flow for active power flow analysis," in *Power Engineering Society General Meeting, 2005. IEEE*, June 2005, pp. 454–459 Vol. 1.

[54] F. Alvarado, "Computational complexity in power systems," *Power Apparatus and Systems, IEEE Transactions on*, vol. 95, no. 4, pp. 1028–1037, July 1976.

[55] U. of Washington, "Power systems test case archive." [Online]. Available: http://www.ee.washington.edu/research/pstca/pf118/pg_tca118bus.htm

[56] EIPP, "Metrics for determining the impact of phasor measurements on power system state estimation," KEMA, Tech. Rep., Jan 2006.

[57] K. Morison, L. Wang, and P. Kundur, "Power system security assessment," *Power and Energy Magazine, IEEE*, vol. 2, no. 5, pp. 30–39, Sept 2004.

[58] D. Fabozzi and T. Van Cutsem, "Localization and latency concepts applied to time simulation of large power systems," in *Bulk Power System Dynamics and Control (iREP) - VIII (iREP), 2010 iREP Symposium*, 2010, pp. 1–14.

[59] B. Stott, "Power system dynamic response calculations," *Proceedings of the IEEE*, vol. 67, no. 2, pp. 219–241, 1979.

[60] J. Undrill, "Structure in the computation of power-system nonlinear dynamical response," *Power Apparatus and Systems, IEEE Transactions on*, vol. PAS-88, no. 1, pp. 1–6, Jan 1969.

[61] P. W. Sauer and M. Pai, *Power System Dynamics and Stability.* Champaign, IL: Stipes Publishing L.L.C., 2006.

[62] Power System Dynamic Performance Committee, "Dynamic models for turbine-governors in power system studies," IEEE Power and Energy Society, Tech. Rep. PES-TR1, Jan 2013.

[63] "Powerworld corporation." [Online]. Available: http://www.powerworld.com/

[64] S.-K. Joo, C.-C. Liu, L. Jones, and J.-W. Choe, "Coherency and aggregation techniques incorporating rotor and voltage dynamics," *Power Systems, IEEE Transactions on*, vol. 19, no. 2, pp. 1068–1075, May 2004.

[65] C. Gear, "Multirate methods for ordinary differential equations," University of Illinois at Urbana-Champaign, Tech. Rep., Sep 1974. [Online]. Available: http://www.osti.gov/scitech/servlets/purl/4254117

[66] M. Crow and J. Chen, "The multirate method for simulation of power system dynamics," *Power Systems, IEEE Transactions on*, vol. 9, no. 3, pp. 1684–1690, 1994.

[67] M. Crow and J. Chen, "The multirate simulation of facts devices in power system dynamics," *Power Systems, IEEE Transactions on*, vol. 11, no. 1, pp. 376–382, 1996.

[68] J. Chen and M. Crow, "A variable partitioning strategy for the multirate method in power systems," *Power Systems, IEEE Transactions on*, vol. 23, no. 2, pp. 259–266, 2008.

[69] M. T. Heat, *Scientific Computing, An Introductory Survey.* New York: McGraw-Hill, 2002.

[70] IEEE Committee Report, "Excitation system models for power system stability studies," *Power Apparatus and Systems, IEEE Transactions on*, vol. PAS-100, no. 2, pp. 494–509, 1981.

[71] J. D. Glover, M. S. Sarma, and T. J. Overbye, *Power System Analysis and Design*. Stamford, CT: Cengage Learning, 2009.